JPn Neuroscience

The Journal of Physiology

J Physiol 591.4 (2013) pp 875–897

Expression of postsynaptic Ca^{2+}-activated K^+ (SK) channels at C-bouton synapses in mammalian lumbar α-motoneurons

Adam S. Deardorff, Shannon H. Romer, Zhihui Deng, Katie L. Bullinger, Paul Nardelli, Timothy C. Cope and Robert E. W. Fyffe

Department of Neuroscience, Cell Biology and Physiology, Wright State University, Boonshoft School of Medicine, Dayton, OH 45435, USA

Key points

- Spinal cord α-motoneurons display strong membrane immunoreactivity (IR) against small-conductance calcium-activated potassium channel (SK) isoform SK2, and a specific subpopulation of motoneurons also express SK3-IR.
- Rat α-motoneurons expressing SK3-IR are significantly smaller, have significantly longer after-hyperpolarization half-decay time, significantly larger after-hyperpolarization amplitude and significantly slower axon conduction velocity than α-motoneurons that lack SK3-IR.
- Motoneuron pools innervating slow-twitch muscles have a higher percentage of SK3-IR α-motoneurons than those innervating fast-twitch muscles.
- Expression of SK3 may contribute to variability in after-hyperpolarization duration and amplitude across different types of rat α-motoneurons and may be a molecular factor differentiating between slow- and fast-type motoneurons.
- In the soma and proximal dendrites of α-motoneurons, large clusters of SK2 and SK3 channel subunits appose cholinergic C-boutons and colocalize with muscarinic type 2 receptors and Kv2.1 channels, which suggests a novel cellular mechanism for state-dependent regulation of neuronal excitability.

Abstract Small-conductance calcium-activated potassium (SK) channels mediate medium after-hyperpolarization (AHP) conductances in neurons throughout the central nervous system. However, the expression profile and subcellular localization of different SK channel isoforms in lumbar spinal α-motoneurons (α-MNs) is unknown. Using immunohistochemical labelling of rat, mouse and cat spinal cord, we reveal a differential and overlapping expression of SK2 and SK3 isoforms across specific types of α-MNs. In rodents, SK2 is expressed in all α-MNs, whereas SK3 is expressed preferentially in small-diameter α-MNs; in cats, SK3 is expressed in all α-MNs. Function-specific expression of SK3 was explored using *post hoc* immunostaining of electrophysiologically characterized rat α-MNs *in vivo*. These studies revealed strong relationships between SK3 expression and medium AHP properties. Motoneurons with SK3-immunoreactivity exhibit significantly longer AHP half-decay times (24.67 *vs.* 11.02 ms) and greater AHP amplitudes (3.27 *vs.* 1.56 mV) than MNs lacking SK3-immunoreactivity. We conclude that the differential expression of SK isoforms in rat and mouse spinal cord may contribute to the range of medium AHP durations across specific MN functional types and may be a molecular factor distinguishing between slow- and fast-type α-MNs in rodents. Furthermore, our results show that SK2- and SK3-immunoreactivity is enriched in distinct postsynaptic domains that contain Kv2.1 channel

A. S. Deardorff and S. H. Romer contributed equally to this work.

© 2012 The Authors. The Journal of Physiology © 2012 The Physiological Society

DOI: 10.1113/jphysiol.2012.240879

clusters associated with cholinergic C-boutons on the soma and proximal dendrites of α-MNs. We suggest that this remarkably specific subcellular membrane localization of SK channels is likely to represent the basis for a cholinergic mechanism for effective regulation of channel function and cell excitability.

(Received 13 July 2012; accepted after revision 31 October 2012; first published online 5 November 2012)
Corresponding author R. E. W. Fyffe: Department of Neuroscience, Cell Biology & Physiology, 202A University Hall, 3640 Col. Glenn Highway, Dayton, OH 45435, USA. Email: robert.fyffe@wright.edu

Abbreviations AHP, after-hyperpolarization; IR, immunoreactivity; mAHP, medium-duration after-hyperpolarization; MN, motoneuron; NeuN, neuronal nuclear protein; SK channel, small-conductance calcium-activated potassium channel; VAChT, vesicular acetylcholine transporter; VGLUT, vesicular glutamate transporter.

Introduction

Small-conductance Ca^{2+}-activated potassium (SK) channels are widely expressed in the mammalian central nervous system (Kohler *et al.* 1996; Tacconi *et al.* 2001; Sailer *et al.* 2004), are activated by nanomolar concentrations of Ca^{2+} through associated calmodulin (Xia *et al.* 1998), and mediate the medium-duration after-hyperpolarization (mAHP) of many brain and spinal cord neurons (Zhang & Krnjević, 1987; Hounsgaard *et al.* 1988; Viana *et al.* 1993; Sawczuk *et al.* 1997; Powers *et al.* 1999; Faber & Sah, 2002, 2003; Sah & Faber, 2002; Bond *et al.* 2004; Miles *et al.* 2005; Faber, 2009). Several homologous SK channel subunits encoded by members of the *KCNN* gene family have been cloned and appear to be distributed in an overlapping pattern in specific neuronal and glial cell populations (Kohler *et al.* 1996; Ishii *et al.* 1997; Stocker & Pedarzani, 2000; Sailer *et al.* 2004; Armstrong *et al.* 2005). Homomeric SK1 ($K_{Ca}2.1$), SK2 ($K_{Ca}2.2$) and SK3 ($K_{Ca}2.3$) channels are (depending on the expression system that is used) highly sensitive to blockade by the bee venom, apamin (Kohler *et al.* 1996; Ishii *et al.* 1997; Shah & Haylett, 2000; Strøbaek *et al.* 2000; Faber & Sah, 2002, 2003; Sah & Faber, 2002). The different channel subunits may interact to form heteromeric channels that result in increased or decreased currents in comparison to homomeric channels (Benton *et al.* 2003; Monaghan *et al.* 2004; Strassmaier *et al.* 2005), although there is still little information about the composition of native channels. The SK channels are expressed in dendrites and dendritic spines in a variety of brain regions, where they are thought to underlie a variety of physiological roles, are subject to cholinergic and adrenergic modulation, and may be involved in mechanisms of synaptic plasticity (Faber *et al.* 2008; Lin *et al.* 2008; Power & Sah, 2008; Lujan *et al.* 2009); however, there is little detailed information about the expression or subcellular localization of SK subunits in spinal cord neurons.

In spinal and hypoglossal motoneurons (MNs), the involvement of SK channels in after-hyperpolarization (AHP) currents is supported by observations that the mAHP is blocked by the SK channel blocker, apamin, as well as by lowering the external calcium concentration or replacing Ca^{2+} with Mn^{2+} ions (Zhang & Krnjević, 1987; Viana *et al.* 1993; Lape & Nistri, 2000). Functionally, mAHP conductances contribute to the modulation of MN discharge rate and, although early studies postulated that they have a role in spike frequency adaptation, other studies indicate that mAHP conductances are non-essential for the early phase of spike frequency adaptation (Baldissera & Gustafsson, 1974; Viana *et al.* 1993; Sawczuk *et al.* 1997; Kernell, 1999; Powers *et al.* 1999; Powers & Binder, 2000; Manuel *et al.* 2005; Meunier & Borejsza, 2005; Miles *et al.* 2005). There are well-documented relationships between mAHP duration and MN size and motor unit type (Burke, 1967; Bakels & Kernell, 1993; Gardiner, 1993). In cat and rat spinal α-MNs, the mAHP is larger and of longer duration in S-type MNs that innervate slow-twitch motor units than in F-type MNs that innervate fast-twitch motor units (Eccles *et al.* 1957; Burke, 1967; Burke *et al.* 1982; Zengel *et al.* 1985; Gardiner, 1993). In contrast, cat γ-MNs display AHPs of variable duration (Kemm & Westbury, 1978). Despite extensive characterization of mAHP properties in S- and F-type α-MNs, it is not known whether the observed mAHP duration and amplitude profiles reflect fundamental differences in SK channel expression, channel activation/deactivation properties, or regulation by neurotransmitters or neuromodulators. To understand more completely the physiological contributions of SK ion channels, it is essential to know the cellular and subcellular distribution of specific channel subunits in different classes of MNs.

Here, we used immunohistochemistry and *in vivo* electrophysiology to investigate the specific distribution and expression patterns of two apamin-sensitive SK channel subunits, SK2 and SK3, in spinal MNs. We demonstrate consistent expression of SK2 in all α-MNs and differential expression of SK3, which is expressed preferentially only in small, presumably S-type, α-MNs. The SK3-expressing α-MNs were shown by electrophysiological analysis to have significantly longer duration, larger amplitude AHPs than MNs that lack SK3. Notably, in contrast to the pattern observed in rat

© 2012 The Authors. The Journal of Physiology © 2012 The Physiological Society

and mouse spinal MNs, all α-MNs in cat spinal cord express SK3 channels. The SK channel immunoreactivity in all α-MNs, regardless of functional type or animal species, is clustered specifically at synapses on the soma or proximal dendrites and is not present in more distal dendrites. Moreover, the postsynaptic SK channels in the perisomatic region are selectively localized at large synapses formed by cholinergic C-boutons. The highly selective localization of large clusters of SK channels at specific sites in the postsynaptic membrane suggests that other molecular signalling and cellular components that are localized at C-bouton synapses, such as muscarinic m_2 receptors and subsurface cisternae, may play key roles in the regulation of SK channel activity and hence of MN firing properties. Indeed, recent investigations have demonstrated that C-bouton activation of m_2 receptors increases motoneuron excitability by reducing the AHP (Miles *et al.* 2007).

Methods

All procedures were performed according to National Institutes of Health Guidelines and approved by the Wright State University Institutional Animal Care and Use Committee. Detailed immunohistochemical analysis of SK channel expression was performed on young adult female (~250 g) Sprague–Dawley rats ($n = 15$), adult female Wistar rats ($n = 20$), adult male or female CBA/J mice (~30 g; $n = 12$), adult female C57/B6 mice ($n = 2$) and adult female cats ($n = 3$). For basic immunostaining procedures and confocal microscopy, all animals were anaesthetized with pentobarbital (150 mg kg^{-1}, I.P.) and transcardially perfused with vascular rinse (0.01 M phosphate buffer with 0.8% NaCl, 0.025% KCl and 0.05% $NaHCO_3$, pH 7.4) followed by 4% paraformaldehyde in 0.1 M phosphate buffer (pH 7.3). For electron microscopy, the fixative solution contained 1% glutaraldehyde (see 'Pre-embedding immuno-electron microscopy' below). Lumbar spinal cord segments were then quickly removed and postfixed in the same fixative for up to 2 h. Tissue was stored in 15% sucrose at 4°C overnight. Transverse sections of L4–L5 lumbar spinal cord were cut on a cryostat at 50–75 μm thick, and then collected in 0.01 M PBS (pH 7.4). When noted, to observe SK2-immunoreactivity (IR) with antigen-retrieval procedures, tissue was incubated in 10 mM sodium citrate, pH 6.0, with 0.05% Tween 20 at 95°C for 20 min prior to immunostaining.

Immunohistochemistry of SK channels

Sections were rinsed with PBS-T (0.01 M PBS containing 0.1% Triton-X, pH 7.3), blocked with normal horse serum (10% in PBS-T), and then incubated in primary antibodies or cocktails of primary antibodies overnight at 4°C. All antibodies were diluted with PBS-T. The SK channel immunoreactivity was localized with polyclonal rabbit anti-SK3 (Chemicon, Temecula, CA, USA; 1:1000 dilution) or polyclonal rabbit anti-SK2 (Alomone, Jerusalem, Israel; 1:100 dilution) directed against amino acid residues 2–21 of human SK3 or against amino acids 542–559 of SK2. The specificity of the primary antibodies has been described (Khanna *et al.* 2001; Tacconi *et al.* 2001; Armstrong *et al.* 2005) and was confirmed here using Western blotting and pre-absorption of the primary antibodies with the peptide antigen. Western blotting of membranes prepared from rat spinal cord tissue and probed with the anti-SK3 antibody revealed that the antibody recognizes a single ~70 kDa molecular weight protein band, and this labelling was abolished by pre-absorption of the antibody with the peptide antigen (Alomone, Jerusalem, Israel; 1 μg peptide/μg antibody); similar specificity and abolition of staining by pre-absorption of the antibody was observed using immunohistochemistry in all three animal species. Similar controls confirmed the specificity of anti-SK2 (which recognizes a single ~72 kDa band in Western blots).

Dual labelling immunohistochemical studies

Double labelling studies were performed by combining one of the anti-SK antibodies with one of the following primary antibodies to detect specific pre- or postsynaptic proteins and their association with SK labelling: anti-synaptophysin (Calbiochem/Oncogene, Darmstadt, Germany; mouse, 1:200 dilution), anti-VAChT (vesicular acetylcholine transporter; Millipore, Billerica, MA, USA; goat, 1:5000 dilution), anti-VGLUT1 and anti-VGLUT2 (vesicular glutamate transporters; Chemicon, Temecula, CA, USA; guinea-pig, 1:5000 dilution), anti-5-HT (Dr J. Pearson Wright State University, Department of Neuroscience, Cell Biology, and Physiology; guinea-pig, 1:5,000), antigephyrin (Alexis, San Diego, CA, USA; mouse, 1:100 dilution) and anti-NeuN (neuronal nuclear protein; Chemicon, Temecula, CA, USA; mouse, 1:500 dilution). Kv2.1 immunohistochemistry was performed using mouse anti-Kv2.1 clone D4/11 at 1:1000 dilution that was developed and/or obtained from the UC Davis/NINDS/NIMH Neuromab facility, supported by NIH grant U24NS0506060 and maintained by the Department of Pharmacology, School of Medicine, University of California (Davis, CA, USA). All primary antibodies were diluted in PBS-T 0.1%, pH 7.4, and incubated overnight at 4°C. The sensitivity and specificity of the primary antibodies against the various synaptic proteins and neuronal markers have been previously described by researchers in our laboratory (Alvarez *et al.* 1997, 1998, 1999; Deng & Fyffe, 2004; Muennich & Fyffe, 2004). Immunoreactivity was detected with species-specific secondary antibodies conjugated to fluorescein isothiocyanate, Cy3 or DyLight 649 (Jackson

© 2012 The Authors. The Journal of Physiology © 2012 The Physiological Society

Immunoresearch, West Grove, PA, USA) diluted 1:50 in PBS-T 0.1%, pH 7.4, and incubated at room temperature for 2–4 h. Given that the antibodies against SK3 and SK2 were raised in the same host species (rabbit), the coexpression studies employed a sequential immunostaining process. The sections were incubated with the first primary antibody (anti-SK3, diluted 1:1000 in 0.01 M PBS-T 0.1%), washed in PBS, and immunoreactive sites revealed with Cy3-conjugated goat anti-rabbit secondary antibody (Fab fragment, 1:50 dilution for 2 h; Jackson Immunoresearch, West Grove, PA, USA). Remaining rabbit IgG binding sites were blocked with an excess of unlabelled Fab fragments (1:10 dilution for 2 h). After washing in PBS to remove unbound Fab fragments, the sections were then incubated in the second primary antibody (anti-SK2, diluted 1:100 in 0.01 M PBS-T 0.1%) and the latter immunogenic sites revealed with fluorescein isothiocyanate-conjugated goat anti-rabbit secondary antibody (1:50 dilution for 30 min). Sections were mounted on gelatin-coated slides and coverslipped in Vectashield mounting medium (Vector Laboratories, Burlingame, CA, USA).

Confocal imaging, analysis and statistics

Images were obtained on a Fluoview 1000 Olympus (Center Valley, PA, USA) confocal microscope with a ×10 objective at 2.0 μm Z-steps, ×20 objective at 1 μm Z-steps, and ×60 oil immersion objective at 0.5 μm steps at 1.0–2.5 digital zoom (NA 1.35). Channel cluster dimensions (maximal diameter and cluster area) and cell sizes (mean soma diameter and cross-sectional area) were measured with ImagePro Plus software (Media Cybernetics, Silver Springs, MD, USA). Immunolabelling was measured using Fluoview software (Olympus). Immunoreactivity for SK3 was considered present if the immunoreactive intensity was at least twofold increased over background. Background intensity was calculated by averaging three randomly sampled areas within the neuropil per image analysed. Significance was set at $P < 0.05$ (SigmaStat; Systat Software, Port Richmond, CA, USA).

Identification of α-MNs

Several approaches and combinations of approaches were used to ensure that α-MNs were adequately differentiated from other ventral horn neurons (γ-MNs and interneurons) during immunohistochemical analysis of SK channel expression. The size of MNs in lumbar spinal cord motoneuron pools has been documented for each mammalian species used here (e.g. Burke *et al.* 1982; Moschovakis *et al.* 1991; Chen & Wolpaw, 1994; Ishihara *et al.* 2001), and our measurements of soma sizes fall within the respective published ranges. Anatomically, MNs were readily distinguished from local interneurons by soma size, morphology, laminar location and Choline Acetyltransferase (ChAT) *vs.* calbindin expression (Carr *et al.* 1998; Alvarez & Fyffe, 2007). For the present study, it was particularly important to distinguish α- from γ-MNs because of the potential for overlap of the soma size distribution of γ- and small α-MNs (Moschovakis *et al.* 1991). We used the recently reported finding that in mouse spinal cord the γ-MNs lack expression of the neuronal nuclear protein NeuN (Friese *et al.* 2009; Shneider *et al.* 2009); our present observations suggest this is also the case in adult mice, rats and cats. Therefore, analysis of NeuN-positive neurons in lamina IX excludes γ-MNs from the sample. Moreover, as described in "specific association of postsynaptic SK3 channels and presynaptic C-boutons", all of the analysed α-MNs received synaptic inputs from large cholinergic C-boutons, which are lacking on γ-MNs (Lagerbäck, 1985; Johnson, 1986; Lagerbäck *et al.* 1986). Various combinations of these strategies gave consistent outcomes and enabled us to focus directly on α-MNs in this study.

Pre-embedding immuno-electron microscopy

For electron microscopy, postperfusion lumbar spinal cord tissue was postfixed overnight at room temperature then stored in 0.01 M PBS (pH 7.3) at 4°C. Tissue sections 50–100 μm thick were cut using a vibratome. Excess aldehydes were blocked with 1% $NaBH_4$, and sections were rinsed thoroughly in PBS. Sections were incubated in polyclonal rabbit anti-SK3 (1:100 dilution in PBS) for 2–4 days at 4°C, and immunostaining was revealed with an ABC-peroxidase kit (Vector Laboratories, Burlingame, CA, USA) using diaminobenzidine (Sigma St. Louis, MO, USA) as the final chromogen (0.02% diaminobenzidine and 0.01% H_2O_2 in 0.05 M Tris buffer) with an 8–10 min reaction time. Reaction products were enhanced using silver intensification, for which sections were treated with 2.5% glutaraldehyde in 0.01 M PBS (30 min), washed three times with Tris–maleic acid buffer, rinsed with nanopure H_2O, and placed in silver nitrate solution (10 min) in a dark room at 60°C. Sections were again rinsed in nanopure H_2O (10 min), after which they were placed in 0.05% gold chloride solution (5 min) at room temperature and rinsed with nanopure H_2O (10 min). Unbound sliver particles were removed by washing in 2.5% sodium thiosulfate (3 min), followed by additional washes in nanopure H_2O and 0.01 M PBS. Sections were postfixed in 2% osmium tetroxide, stained *en bloc* with 1.0% uranyl acetate, dehydrated in a graded series of ethanols, cleared through two 5 min washes in propylene oxide, infiltrated with 1:1 propylene oxide–Epon-Araldite, and finally flat-embedded in Epon-Araldite between two Teflon-coated coverslips. Small areas containing immunolabelled motoneurons were selected from the sections and glued onto a resin block. Ultrathin sections (60–70 nm)

© 2012 The Authors. The Journal of Physiology © 2012 The Physiological Society

were obtained on a Sorvall MT 6000 ultramicrotome (Dupont Company, Newtown, CT, USA) and collected serially on copper grids coated with a thin layer of Formvar, counterstained with uranyl acetate and lead citrate (5 min), and viewed on a Philips EM201 transmission electron microscope (Philips Electron Optics, Amsterdam, Netherlands) equipped with a Gatan digital camera (Gatan Inc, Pleasanton, CA, USA). Digital images were used for synaptological survey of the neuron surface and the determination of synapse type and distribution of immunoreactivity. Electron micrographs were produced in CorelDRAW (Corel Corp., Ottawa, Ontario, Canada) from standard electron microscopy negative plates that were scanned at 200 d.p.i.

In vivo electrophysiology

Twenty female Wistar rats were studied in single terminal recording sessions. Deep anaesthesia (absent withdrawal and corneal reflex) was induced by isoflurane (4–5% in 100% O_2, by inhalation in an induction chamber) and maintained by isoflurane (1–3% in 100% O_2, by inhalation through a tracheal cannula). The animal was monitored for respiratory rate (40–60 breaths min^{-1}), end-tidal CO_2 (3–5%), oxygen saturation (>90%), heart rate (300–500 beats min^{-1}) and core temperature (36–38°C). These levels were variously maintained by adjusting the isoflurane concentration and radiant heat sources and by scheduled subcutaneous injection of Ringer–dextrose solution. In some cases, adequate recording stability required intraperitoneal injection of a muscle relaxant drug (pancuronium bromide 0.2 mg kg^{-1}).

Standard procedures were used to prepare the spinal cord and left hindlimb for electrophysiological stimulation and recording, with the animal secured in a rigid frame (Seburn & Cope, 1998; Haftel *et al.* 2004, 2005; Bullinger *et al.* 2011). The left tibial nerve was carefully dissected free of other tissues and suspended on a monopolar, silver stimulating electrode. Other hindlimb nerves were crushed, including the common peroneal nerve and sural nerves. Dorsal exposure of the lumbosacral spinal cord (L4–S1) by laminectomy and longitudinal incision of the dura mater provided access to dorsal roots L4 and L5, which were carefully dissected free of surrounding tissue and suspended in continuity on bipolar silver hook electrodes for recording, and tibial motoneurons via dorsolateral penetration of the spinal cord. Skin flaps were used to construct pools for bathing all exposed tissues with warm mineral oil.

In vivo intracellular recordings were made from antidromically identified tibial α-MNs using glass microelectrodes (~10–25 MΩ) filled with 10% neurobiotin (Vector Laboratories, Burlingame, CA, USA) and 5% 488 dextran (Invitrogen, Grand Island, NY, USA) in 0.1 M Tris-OH and 1.0 M potassium acetate. Only those MNs with stable membrane potential and with action potential amplitude >60 mV were deemed acceptable for further study. Failure to meet these criteria accounts for the incomplete data set obtained from some MNs. Motoneurons were injected with current through the micropipette in order to measure the following intrinsic electrical properties as previously reported in our laboratory (e.g. Bullinger *et al.* 2011): rheobase current (depolarizing pulses, 50 ms in duration, at the lowest strengths capable of initiating action potentials from the resting membrane potential), AHP (following individual action potentials generated by suprathreshold pulses, 0.5 ms in duration), input resistance (from hyperpolarization produced by −1 and –3 nA current pulses, 50 ms in duration) and axon conduction velocity (antidromic conduction delay divided by tibial nerve length). In some animals, tibial nerve lengths and thus conduction velocity were not measured. Following physiological characterization, motoneurons were labelled by intracellular injection of 10% neurobiotin with 5% dextran in Tris Buffer (0.1M Tris-OH, 1M Potassium Acetate, PH 7.6). Positive current pulses (5 nA), delivered as 400-ms-long pulses at 2 Hz for 2–5 min, were used to aid neurobiotin passage into the motoneuron. Records of MN membrane potential and electrode current were collected, digitized (20 kHz), stored and analysed with CED Power 1401 and CED Spike2 software (Cambridge Electronic Design, Cambridge, UK).

After data collection, animals were killed by an intraperitoneal overdose of pentobarbital (150 mg kg^{-1} I.P.) and perfusion fixed as described in above methods. Spinal segments containing intracellularly labelled motoneurons were postfixed overnight. Serial transverse sections (75 μm thick) were obtained on a vibrating microtome and were initially examined for dextran immunofluorescence using a fluorescence dissecting microscope. Those sections containing intracellularly labelled motoneurons were serially processed for SK3 immunoreactivity as described in "immunohistochemistry of SK channels". To enhance intracellular labelling, neurobiotin was visualized with 488 streptavidin (Invitrogen; diluted 1:1000 in 0.01 M PBS containing 0.1% Triton X for 2 h at room temperature).

Figure composition

Figures were composed using CorelDRAW (version 12.0). Graphs were composed in SigmaPlot (version 9.0, Systat Software; SPSS Inc, Chicago, IL, USA). Microscope image modifications for presentation, such as adjusting contrast and brightness, were carried out in Image Pro Plus (Media Cybernetics, Bethesda, MD, USA) and always preserved all the information content of the images. Some images were sharpened using a 'high-gauss' filter. Quantification was always carried out using original unprocessed images.

© 2012 The Authors. The Journal of Physiology © 2012 The Physiological Society

Results

Immunoreactivity for SK2 and SK3 (SK-IR) was observed in all laminae of the lower lumbar spinal cord, consistent with previous immunohistochemical surveys of SK channel expression (Sailer *et al.* 2004; Mongan *et al.* 2005). The highest levels of SK-IR were evident in the superficial dorsal horn and in the medial and lateral motoneuron pools in lamina IX of the ventral horn (Fig. 1). Whilst immunoreactivity for both SK2 and SK3 was detected throughout the spinal cord grey matter, the overall intensity of SK2 immunolabelling was generally lower than that observed for SK3 and, with the fixation conditions used in our experiments, the detection of SK2-IR was more effective and consistent in mouse and rat tissue compared with cat tissue. Within a single tissue section, SK3-IR, when observed at all, could vary in intensity from modest (two to three times background) to strong (more than three times background) levels between individual neurons; however, all SK3-positive neurons, regardless of

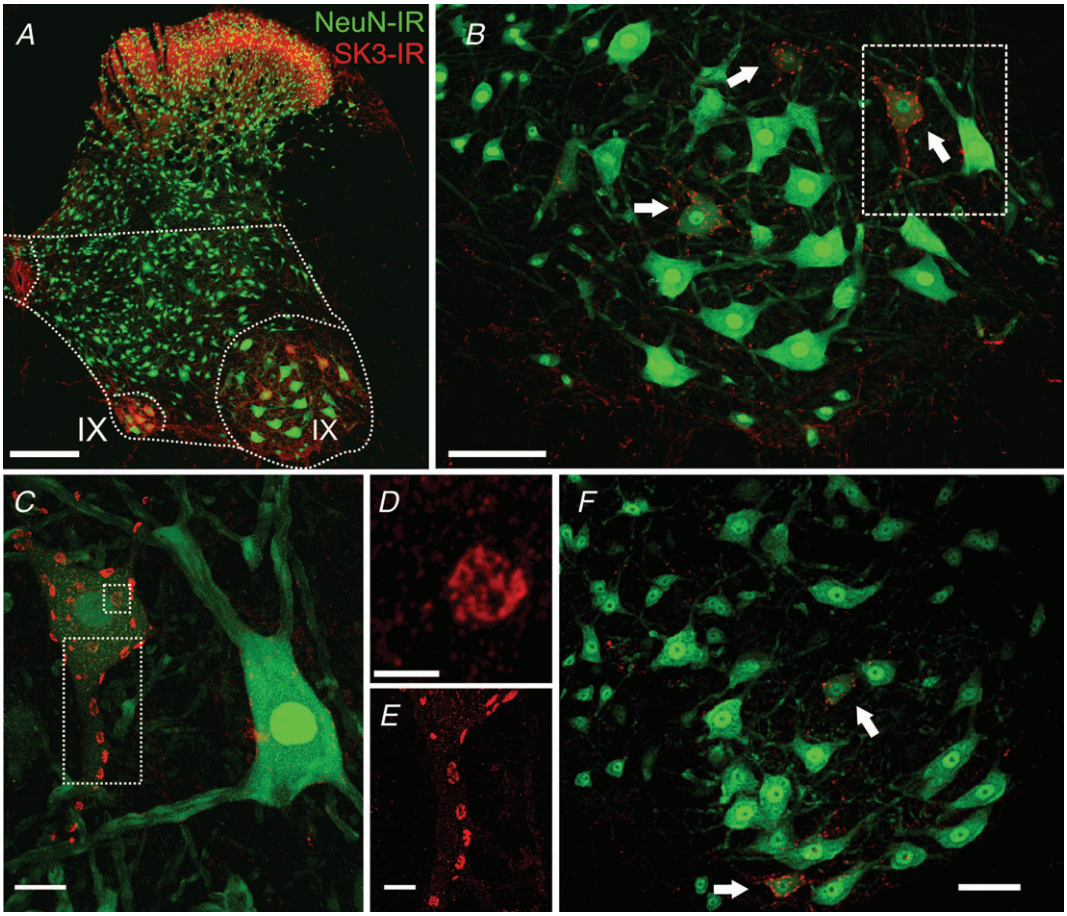

Figure 1. Differential expression of small-conductance calcium-activated potassium channel 3 (SK3) immunoreactivity (IR) in rat and mouse lumbar spinal motoneurons (MNs)
Images are representative micrographs from confocal stacks exhibiting SK3-IR (red) and NeuN-IR (green) in coronal sections of spinal cord. *A–E* are from a rat, and *F* is from a mouse. *A–E* show successively higher magnification views (×10–×60 objectives, plus digital zoom in *D* and *E*) of the lateral lamina IX region outlined in panel *A*. *A*, strong SK3 immunoreactivity is observed in the superficial dorsal horn and in medial and lateral lamina IX areas of the ventral horn as indicated (12 superimposed optical sections,1.0 μm Z-step; scale bar represents 200 μm). *B*, in the lateral MN pool, arrows point to three smaller MNs expressing SK3-IR. Frequently, MNs expressing SK3-IR have less intense NeuN-IR compared with the majority of MNs (six optical sections; scale bar represents 100 μm). *C*, in SK3-expressing MNs, clustered SK3-IR is distributed in a mosaic pattern on the perisomatic membrane and proximal dendrites (30 optical sections, 0.5 μm Z-step; scale bar represents 20 μm). *D*, high-power micrograph of *en face* cluster depicted in the small square dotted box in *C*. Individual SK3-IR clusters display complex substructure and appear to be composed of multiple small regions of intense immunoreactivity. Image is a single optical confocal section. Scale bar represents 5 μm. *E*, SK3-IR clusters on a proximal dendrite (rectangular dotted area demarcated in *C*; 25 optical sections (0.5 μm Z-step; scale bar represents 10 μm). *F*, similar to the expression pattern seen in *B*, SK3-IR in mouse MNs is exhibited in a subset of MNs in the lateral MN pools; 13 optical sections (1.0 μm Z-step; scale bar represents 50 μm).

© 2012 The Authors. The Journal of Physiology © 2012 The Physiological Society

signal intensity, were grouped together for analysis and comparison against neurons that lacked SK3 completely. In ventral horn neurons, SK-IR appeared to be largely surface membrane associated and was concentrated in 'hot spots' that outline the perisomatic surface of MNs (soma and proximal dendrites); punctate labelling was also distributed throughout the neuropil of the ventral horn.

Immunoreactivity for SK3 in motoneurons

In mice and rats (Fig. 1) and in cats (Fig. 2), SK3-IR was concentrated in disc-shaped patches distributed in a mosaic pattern on the soma and proximal dendrites of MNs. In proximal dendrites (up to 100 μm from the soma), SK3-IR was easily resolved (e.g. Fig. 1*C*; see also Fig. 6*A*), but we did not observe any SK3-IR associated with more distal dendrites. The large, intensely labelled juxtasomatic channel cluster domains were analysed quantitatively using fluorescence confocal microscopy (Muennich & Fyffe, 2004). The surface areas of the SK3-IR channel clusters in mouse MNs ranged from 1.28 to 11.63 μm^2, with a mean of 5.02 μm^2 (SD $\pm$ 1.79) and mean diameter of 2.34 μm (Fig. 3). The surface areas of the SK3-IR channel clusters in rat MNs ranged from 2.07 to 32.98 μm^2, with a mean of 9.80 μm^2 (SD $\pm$ 4.32) and mean diameter of 3.58 μm (Fig. 3). The surface areas of the SK3-IR channel clusters in cat MNs ranged from 6.16 to 67.34 μm^2, with a mean of 25.91 μm^2 (SD $\pm$ 11.63) and mean diameter of 5.55 μm (Fig. 3). Noticeably, most of the SK3-IR in MNs was concentrated in patches greater than 1.0 μm^2. The lack of small clusters is not due to inability to detect or measure smaller clusters. Our previous studies of Kv2.1 channel distribution in motoneurons demonstrates the capability of our methods to measure smaller sized patches of immunoreactivity quantitatively (Muennich & Fyffe, 2004), and small punctae of SK-IR were observable in other spinal neurons in the present experiments. As previously noted for large Kv2.1 channel clusters, when individual SK3 membrane clusters are examined at high resolution they display a complex substructure that represents a non-uniform aggregation of much smaller structures (Fig. 1*D*). For SK3-IR, in contrast to Kv2.1-IR at the same location, there was a tendency for immunostaining to be more concentrated around the periphery of the cluster region (see also Fig. 12).

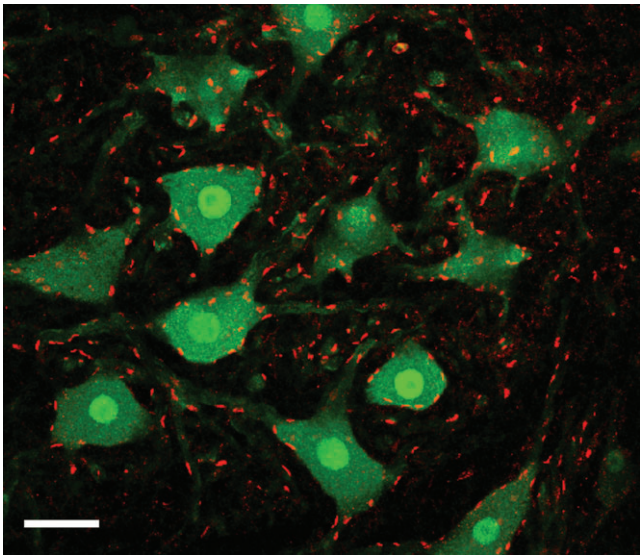

Figure 2. Small-conductance calcium-activated potassium channel 3 immunoreactivity is present in all cat lateral lumbar spinal motoneurons
In contrast to the rat and mouse (Fig. 1), clusters of intense SK3-IR are observed in every MN in the pool (confocal image stack is 13 optical sections, 1.0 μm Z-step; scale bar represents 50 μm).

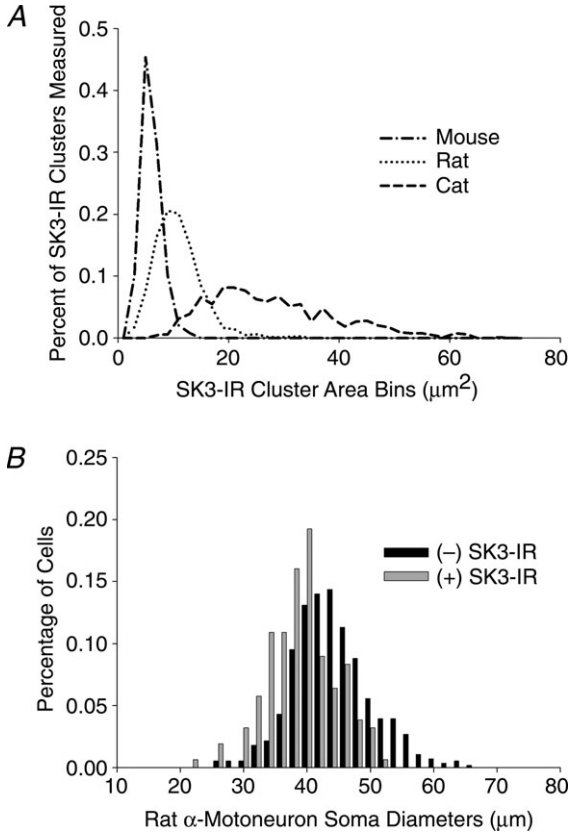

Figure 3. Distribution of SK3-IR cluster areas and motoneuron soma sizes
A, the lines represent the distribution (calculated in increments of 2 μm^2; total range 1–73 μm^2) of SK3-IR cluster sizes on lumbar MNs in different species. The mean areas for cluster sizes were 5.02 μm^2 for mice (n = 247), 9.80 μm^2 for rats (n = 1497) and 25.91 μm^2 for cats (n = 639). *B*, in rats, MNs with positive SK3-IR had a mean soma diameter of 38.11 $\pm$ 5.39 μm (SD; n = 156) whereas MNs that lack SK3-IR had a mean soma diameter of 42.994 $\pm$ 6.36 μm (SD; n = 557). The two populations are significantly different (Student's unpaired t test, $P < 0.0001$).

© 2012 The Authors. The Journal of Physiology © 2012 The Physiological Society

Sparsely distributed punctae of SK3-IR were observed throughout the neuropil in laminae IX and VII, in addition to immunoreactivity that could be clearly associated with individual proximal dendrites. Like the prominent juxtasomatic clusters of immunoreactivity, labelling in the neuropil was abolished in the presence of pre-incubated antigen, indicating a high degree of specificity in the observed fluorescence signal. Although these punctae could potentially represent SK expression in more distal dendrites of MNs (Li & Bennett, 2007), the cellular localization of this labelling remains undetermined, because even when distal dendrites of intracellularly labelled MNs were resolved and analysed in detail, they lacked SK3 expression in any branches more than approximately 150–200 μm from the soma.

Differential expression of SK3-IR in small *vs.* large motoneurons in rats and mice

In rats and mice, SK3-IR clusters were present in discrete populations of MNs (Fig. 1*B* and *F*), whereas in cats the SK3-IR was observed in all presumed α-MNs (Fig. 2). In the lateral MN pools of rat lumbar cord, 20% (254 of 1267 NeuN-positive neurons) of NeuN-labelled MNs expressed SK3 immunoreactivity in the surface membrane. In mice, 17% (95 of 557 neurons) of the MNs expressed SK3.

Typically, NeuN labelling was present in the cytoplasm of the cell body and proximal dendrites as well as in neuronal nuclei, but there was a clear qualitative and quantitative difference in the level of NeuN immunostaining among cell bodies of neurons in the lateral lamina IX MN pools of both the rat and mouse spinal cord. These differences permit classification of α-MNs into two categories that reflect a direct relationship between soma size and pattern of NeuN expression. Neurons in one group, compromising the majority of α-MNs in each MN pool (Fig. 1*B* and *F*), exhibit well-stained nuclei and diffuse cytoplasmic labelling that appears relatively intense and clearly extends into the proximal dendrites of the neuron. In contrast, other NeuN-positive α-MNs have well-stained nuclei but exhibit weak cytoplasmic labelling. Neurons in the latter class appear to be of smaller size than the former.

Of particular interest is the fact that the strongest levels of SK3-IR in surface membrane clusters was restricted to the α-MN population that exhibited a low level of cytoplasmic NeuN labelling (Fig. 1*B*, *C* and *F*). Motoneurons that expressed relatively high cytoplasmic levels of NeuN generally lacked SK3-IR, although a few such neurons expressed SK3 at modest levels. In the rat, the mean soma diameter of SK3-expressing MNs ($n = 156$), regardless of NeuN labelling intensity, was 38.11 ± 5.39 μm (SD), which was significantly smaller ($P < 0.0001$) than that of MNs ($n = 557$) that lacked detectable SK3-IR clusters, 42.99 ± 6.36 μm (SD; Fig. 3*B*). A similar result was obtained when the cross-sectional areas of the cell bodies were compared. The mean cross-sectional areas for SK3-IR MNs ($n = 61$) was 1066.2 ± 179.2 μm^2, compared with 1263.6 ± 205.1 μm^2 for MNs ($n = 183$) that lacked SK3-IR ($P < 0.01$). Although there were other, much smaller, unidentified, but NeuN positive (and therefore unlikely to be γ-MNs), neurons interspersed among the neurons of the MN pool, these small neurons lacked SK3-IR and were presumed, based on morphology and the lack of C-bouton synaptic contacts, to be interneurons.

All rat and mouse motoneurons express SK2 channels

Given that large-diameter MNs do not appear to express SK3, we performed dual staining of SK2 and SK3 through the use of Fab fragments to double label sections with primary antibodies from the same host, in order to determine whether the large-diameter MNs express SK2 and/or if SK2 and SK3 are coexpressed in the small MNs. The results showed that SK2 and SK3 were coexpressed in the small MNs and that SK2 was expressed in large MNs lacking SK3-IR in both rats (Fig. 4) and mice. Like SK3, SK2-IR appeared to be organized in a cluster pattern over the surface membrane of the soma and proximal dendrites and appeared to colocalize with SK3 in SK3-IR MNs. The individual antibody peptide sequences were highly specific to each of the SK isoforms, and peptide pre-incubation studies for each of the two antibodies did not affect the immunoreactivity of the alternate isoform (data not shown), suggesting that there was no cross-reactivity between the antibodies. The fact that every MN was accounted for as either SK2-IR or SK2- and SK3-IR suggests that the lack of SK3-IR in large motoneurons was not caused by antibody penetration problems or other technical issues.

The pattern of SK3 expression in physiologically identified rat motoneurons in lateral motoneuron pools

It is widely accepted, on the basis of correlations between measurements of rheobase, input resistance, axonal conduction velocity and total membrane surface area, that small MNs innervate slow-twitch muscle fibres, while large MNs innervate fast-twitch muscle fibres (Henneman & Olson, 1965; Henneman *et al.* 1965*a*,*b*; Burke, 1967; Burke *et al.* 1982; Zengel *et al.* 1985; Gardiner, 1993). Given the smaller size of SK3-IR cells, we injected retrograde tracer into specific hindlimb muscles to label MNs for *post hoc* analysis of SK3-IR. Approximately 25% (37 of 149 MNs analysed) of MNs innervating the predominately fast-twitch medial and lateral gastrocnemius muscles (MG/LG) were SK3-IR, while 63% (84 of 133) of MNs innervating the predominately slow-twitch soleus muscle were SK3-IR (Fig. 5).

© 2012 The Authors. The Journal of Physiology © 2012 The Physiological Society

Apamin-sensitive SK currents underlie the motoneuron AHP (Zhang & Krnjević, 1987; Viana *et al.* 1993; Li & Bennett, 2007), and it has been suggested that AHP half-decay time accurately distinguishes fast- from slow-twitch motor units (Eccles *et al.* 1957; Zengel *et al.* 1985; Gardiner & Kernell, 1990; Gardiner, 1993). Therefore, in a separate set of experiments, rat tibial MNs were electrophysiologically characterized, intracellularly labelled with neurobiotin, and analysed for SK3-IR (Fig. 6). Compared with MNs not expressing SK3, SK3-IR MNs showed a significantly longer AHP half-decay time (24.2 ± 4.7 (SD; $n = 8$) *vs.* 11.0 ± 1.8 ms (SD; $n = 27$), Student's unpaired *t* test, $P < 0.001$; Fig. 6*A*) and significantly greater AHP amplitude as measured from resting membrane potential (3.1 ± 1.3 (SD; $n = 8$) *vs.* 1.5 ± 1.0 mV (SD; $n = 27$), Student's unpaired *t* test, $P = 0.001$; Fig. 7*A*). In most analysed cells, the resting membrane potential was well documented throughout the recording period, and it was observed that there was no significant difference between individual cells

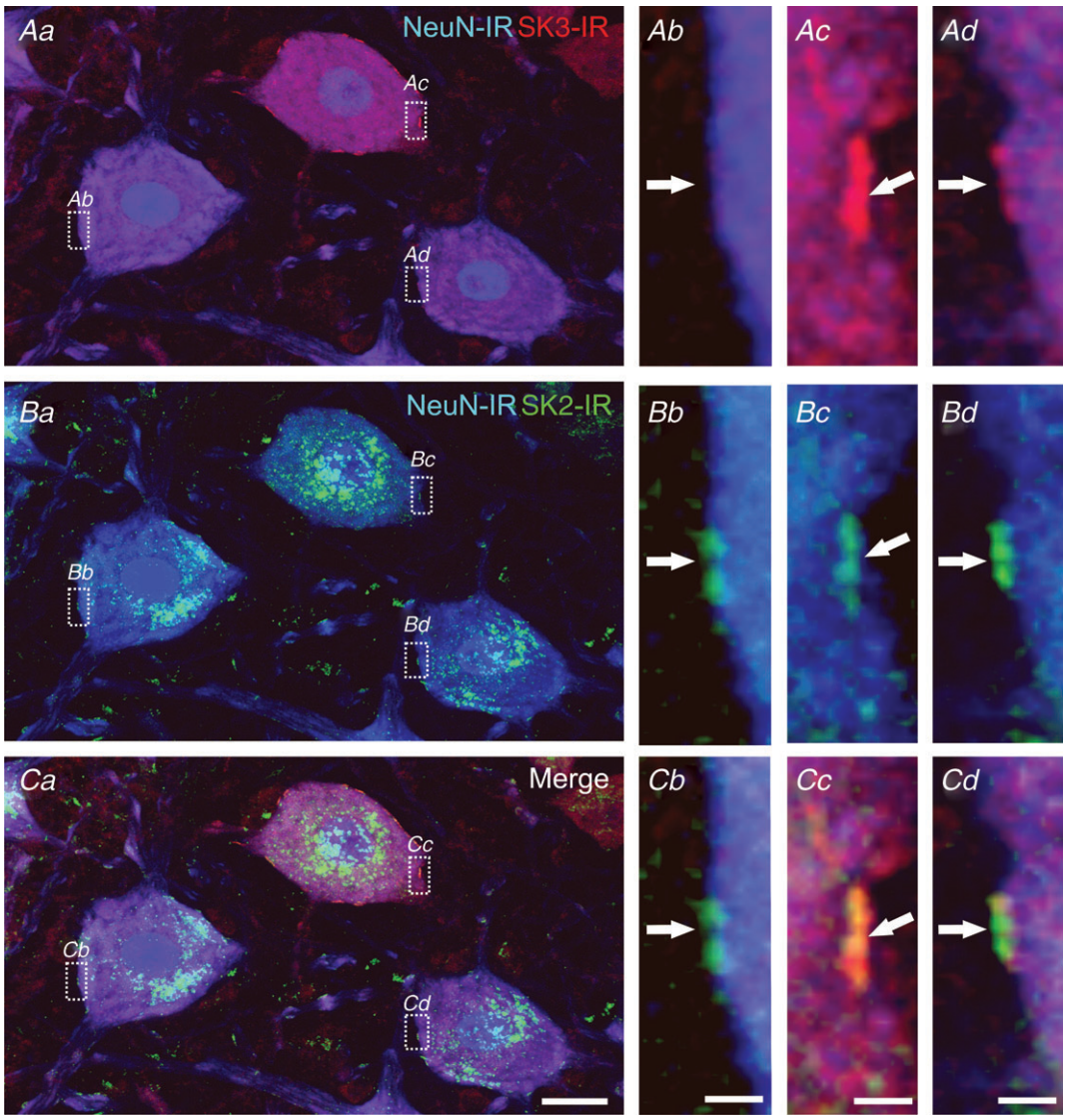

Figure 4. Differential expression of SK3-IR and SK2-IR in rodent lumbar spinal α-motoneurons
Aa, *Ba* and *Ca* are images of the same region showing three adjacent MNs (eight optical sections, 1.0 μm Z-steps; scale bar in *Ca* represents 20 μm) and respective SK3-IR (red), SK2-IR (green) and NeuN labelling (blue). Surface membrane regions (boxed areas in *Aa*, *Ba* and *Ca*) from each MN are shown at high magnification (scale bars represent 2.0 μm) in the three right-hand panels. Two of the neurons (see boxed areas *Ac* and *Ad*) have intense (more than three times background, *Ac*) or moderate (more than two times background, Ad) clusters of SK3-IR (arrows), but SK3-IR is absent from the third MN (*Ab*). All three neurons express SK2-IR at the same sites (arrows in *Bb*, *Bc* and *Bd*). In MNs that express both SK2 and SK3, the immunostaining is clearly colocalized at these sites (merged images in *Cc* and *Cd*).

© 2012 The Authors. The Journal of Physiology © 2012 The Physiological Society

(SK3-positive cells ($n = 7$), -53.4 ± 4.8 mV (SD); and SK3-negative cells ($n = 21$), -56.3 ± 8.2 mV, Student's unpaired t test, $P = 0.39$). Moreover, SK3-expressing MNs had a significantly greater input resistance (3.1 ± 0.5 (SD; $n = 4$) *vs.* 1.7 ± 1.1 MΩ (SD; $n = 15$), Student's unpaired t test, $P = 0.035$) and a significantly slower axon conduction velocity (44.2 ± 9.1 (SD; $n = 7$) *vs.* 58.6 ± 5.1 m s^{-1} (SD; $n = 21$), Student's unpaired t test, $P < 0.001$; Fig. 7*A*) than MNs not expressing SK3. No significant difference in mean rheobase was observed between cell types (SK3-positive cells ($n = 9$), 3.8 ± 3.3 nA (SD); and SK3-negative cells ($n = 27$), 8.8 ± 7.3 nA (SD), Student's unpaired t test, $P = 0.55$; Fig. 7*A*), although the observed values indicate a trend towards SK3 being present in 'electrically smaller' MNs.

We observed the normal tendency for AHP half-decay time to co-vary with AHP amplitude ($r = 0.61$, $P < 0.001$; Fig. 7*B*) and, as in previous studies (Eccles *et al.* 1958; Bakels & Kernell, 1993; Prather *et al.* 2011), we observed a weak but significant negative correlation between rheobase current and AHP half-decay time ($r = -0.39$, $P = 0.028$; Fig. 7*B*) and a stronger negative correlation between axon conduction velocity and AHP half-decay time ($r = -0.85$, $P < 0.001$; Fig. 7*B*). In the plots shown in Fig. 7, the data points representing SK3-expressing MNs cluster in regions of the overall parameter distribution that are typically represented by MNs innervating slow-twitch motor units in rats (Gardiner, 1993; Bakels & Kernell, 1993).

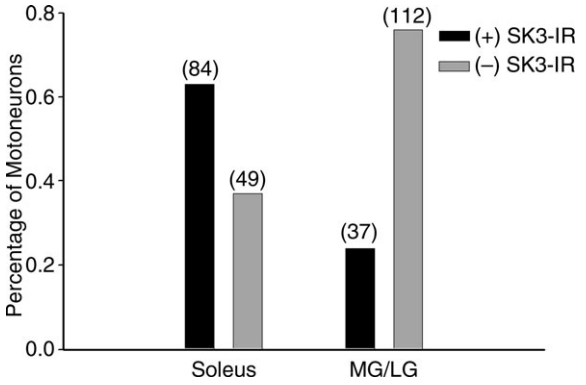

Figure 5. Motoneuron pools innervating slow-type muscles have a higher percentage of motoneurons with SK3-IR
Rat MN pools were retrogradely labelled with fluorogold from intramuscular injections into either the soleus (predominately S-type muscle) or the medial and lateral gastrocnemius (MG/LG; predominately F-type muscle). *Post hoc* analysis of labelled MNs classified SK3 expression as either (+)SK3-IR (more than two times background) or (–)SK3-IR (undetectable immunoreactivity). The number of MNs sampled is listed in parentheses. Approximately 63% of MNs innervating the S-type soleus muscle have (+)SK3-IR profiles and approximately 25% of MNs innervating the F-type MG/LG muscles have (+)SK3-IR. The proportion of SK3-expressing neurons in each pool is significantly different as revealed by Z-test ($P < 0.001$).

For all MNs analysed in this study, the mean AHP amplitude (1.9 ± 1.2 mV (SD; $n = 35$)), mean AHP half-decay time (14.0 ± 6.2 ms (SD; $n = 35$)), mean input resistance (2.0 ± 1.2 MΩ (SD; $n = 19$)) and mean conduction velocity (55.0 ± 8.8 m s^{-1} (SD; $n = 28$)) are consistent with the average values previously published (Bakels & Kernell, 1993; Seburn & Cope, 1998; Bichler *et al.* 2007*a*,*b*; Bullinger *et al.* 2011). In order to have an adequate sample for comparative analysis of SK3-expressing MNs, which are a minority of the total α-MN population, we necessarily biased our sample towards small, low-rheobase cells. As a result, the mean rheobase current for all α-MNs analysed in this study (7.5 ± 6.8 nA (SD; $n = 36$)) is slightly lower than previously reported by researchers our laboratory in female Wistar rats anaesthetized with isoflurane (Bullinger *et al.* 2011), but still falls within ranges typical for anaesthetized rat α-MNs (Seburn & Cope, 1998; Bichler *et al.* 2007*a*,*b*).

Postsynaptic localization of SK3 channels

Double labelling with antibodies against the synaptic protein synaptophysin revealed a close apposition between the sites of presynaptic inputs (synaptophysin-labelled boutons) and postsynaptic clusters of the SK channel (Fig. 8). In each mammalian species we analysed, every postsynaptic SK3-IR cluster was closely apposed by a synaptophysin-labelled bouton, although clearly not all presynaptic boutons on the MN surface were opposed to SK3 clusters. Similar results were observed for SK2 clusters. Although superimposed images of stacked optical sections occasionally showed a thin band of overlapping immunostaining (Fig. 8), this labelling appearance was consistent with earlier observations of membrane channel labelling at synapses in MNs in which clear ultrastructural verification of apposed pre- and postsynaptic markers were obtained (Muennich & Fyffe, 2004).

Our electron microscopic analysis (Fig. 9) supports the conclusion that the SK channel clusters are postsynaptically localized in the surface membrane of MNs and that there is generally very little SK protein, if any, present in the presynaptic boutons apposed to the MN soma or proximal dendrites. The postsynaptic SK clusters appeared to be apposed predominantly by the largest presynaptic boutons surrounding the soma (Fig. 8). As a result of their size, these large boutons were likely to be C-boutons (Conradi *et al.* 1979), and this hypothesis was tested by use of markers for cholinergic synapses.

Specific association of postsynaptic SK3 channels and presynaptic C-boutons

Cholinergic synapses in the ventral horn were revealed by immunoreactivity against the vesicular acetylcholine

© 2012 The Authors. The Journal of Physiology © 2012 The Physiological Society

transporter (VAChT), which labels distinct populations of cholinergic axon terminals, including those arising from motor axon collaterals in ventral lamina VII (that contact Renshaw cells), as well as large C-boutons that uniquely contact the soma and proximal dendrites of α-MNs in lamina IX (Alvarez *et al.* 1999; Hellström *et al.* 2003; Deng & Fyffe, 2004; Miles *et al.* 2007; Zagoraiou *et al.* 2009). Dual labelling of SK3 and VAChT (Fig. 10) demonstrated consistent association of motoneuron SK3-IR clusters and large VAChT-IR presynaptic C-boutons (94.9% correspondence; $n = 1051$ SK3-IR clusters); i.e. almost every cluster of SK-IR on the membrane surface of an SK3-expressing MN, including SK3 in proximal dendrites, was closely apposed by a cholinergic nerve terminal.

To confirm specificity and selectivity of the association of the postsynaptic SK clusters with cholinergic inputs, we also analysed SK3-IR in conjunction with markers for glutamatergic, monoaminergic and glycine/GABAergic synapses (Fig. 11). In contrast to the striking relationships between VAChT-IR boutons and SK3-IR demonstrated in Fig. 10, populations of glutamatergic boutons revealed by immunostaining against two different isoforms of the vesicular glutamate transporter (VGLUT1 and VGLUT2; Alvarez *et al.* 2004, 2011) were not associated with SK-IR sites. Likewise, despite dense monoaminergic innervation of the ventral horn MNs (Alvarez *et al.* 1998), no appositions were observed between 5-HT-immunoreactive terminals and SK3 clusters. Finally, there was no overlap or relationship between SK3-immunoreactivity and immunostaining for gephyrin, a postsynaptic scaffolding protein present at inhibitory glycinergic and GABAergic synapses on MNs (Alvarez *et al.* 1997).

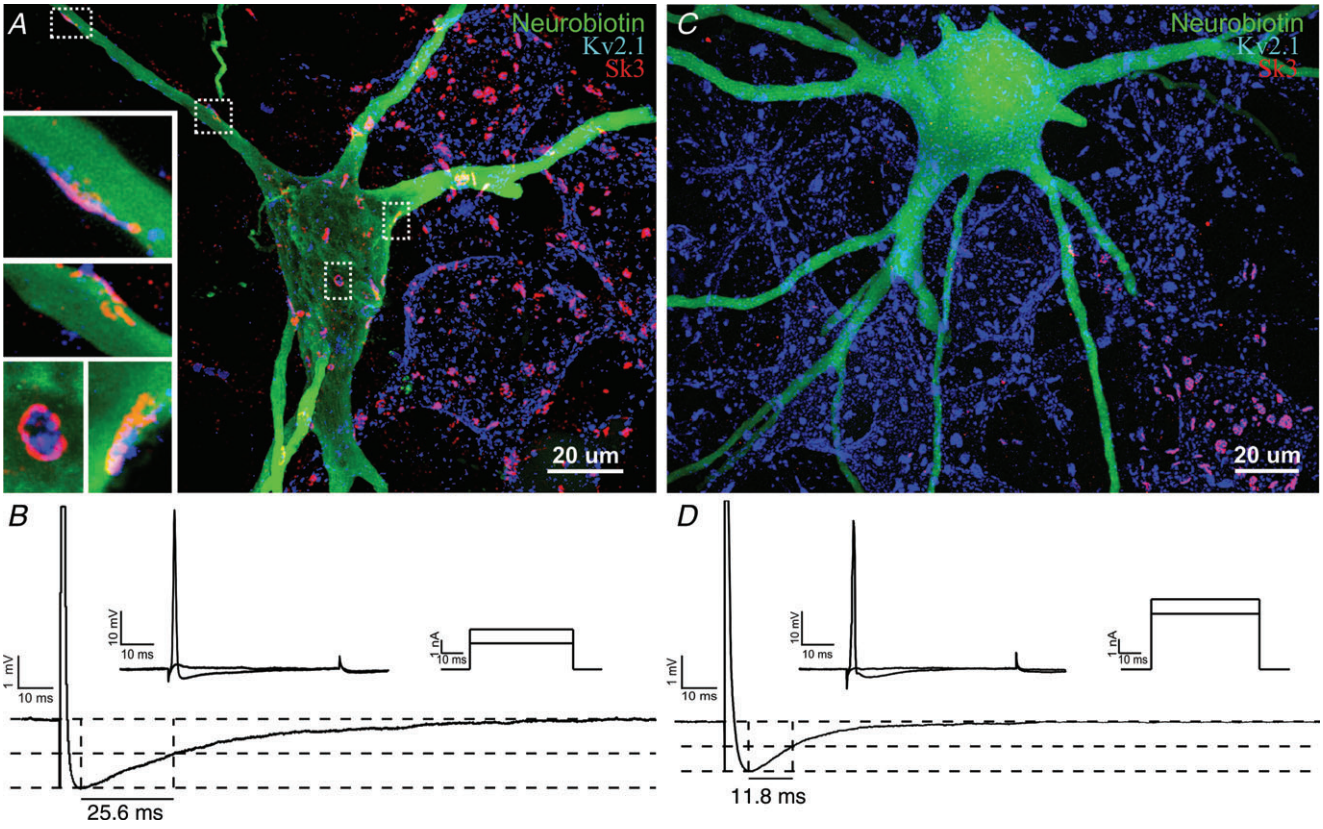

Figure 6. Expression of SK3 in physiologically characterized α-motoneurons
Tibial MNs were electrophysiologically characterized, labelled with neurobiotin and analysed for SK3 expression using *post hoc* immunohistochemistry. *A*, an SK3-expressing tibial motoneuron, with high-magnification images (insets) of clusters on the soma and proximal dendrites. The image in *A* is 85 optical sections (0.5 μm Z-step). Insets are four to eight optical sections (0.5 μm Z-step). *B*, intracellular physiological recordings from the same neuron. Upper traces in *B* show rheobase current injections (upper right) and corresponding voltage records (upper left); rheobase current in this cell, i.e. the minimal current eliciting an action potential, is 3 nA. The lower trace shows the after-hyperpolarization (AHP; half-decay time = 25.56 ms, amplitude = 2.01 mV; average of 45–60 trials; action potential amplitude is truncated to highlight AHP). *C* and *D*, similar image and recordings (taken at a matching resting membrane potential, ~48 mV, to those in *B*) of a tibial motoneuron that does not express SK3. Image in *C* is 90 optical sections (0.5 μm Z-step). For the cell in *C*, rheobase current is 4 nA. After-hyperpolarization half-decay time is 11.83 ms and AHP amplitude is 1.5 mV (average of 45–60 trials).

© 2012 The Authors. The Journal of Physiology © 2012 The Physiological Society

Colocalization of SK and Kv2.1

We have previously demonstrated that Kv2.1 channel-IR is present in a characteristic mosaic pattern of large and small ion channel clusters in α-MNs, with the largest clusters being located postsynaptically at C-bouton synapses (Muennich & Fyffe, 2004; Wilson *et al.* 2004). We used double labelling with anti-SK and anti-Kv2.1 antibodies to determine whether these respective channel properties were colocalized together at the large C-bouton synapses (Fig. 12). The illustrated data focuses on SK3-IR in rat spinal cord, but equivalent results were obtained for both SK isoforms in rats and mice. There was a clear and consistent colocalization between SK-IR and Kv2.1-IR at the large cluster sites in α-MNs, with the respective SK3-IR and Kv2.1-IR signals interdigitating to 'fill' the space demarcated by the cluster region (Fig. 12). In most cases, including those illustrated at high magnification in Fig. 12, the SK3-IR tended to be located more towards the periphery of the cluster region, surrounding the Kv2.1-IR, consistent with the fact that the average size of SK3 clusters is larger than that of Kv2.1 clusters (Muennich & Fyffe,

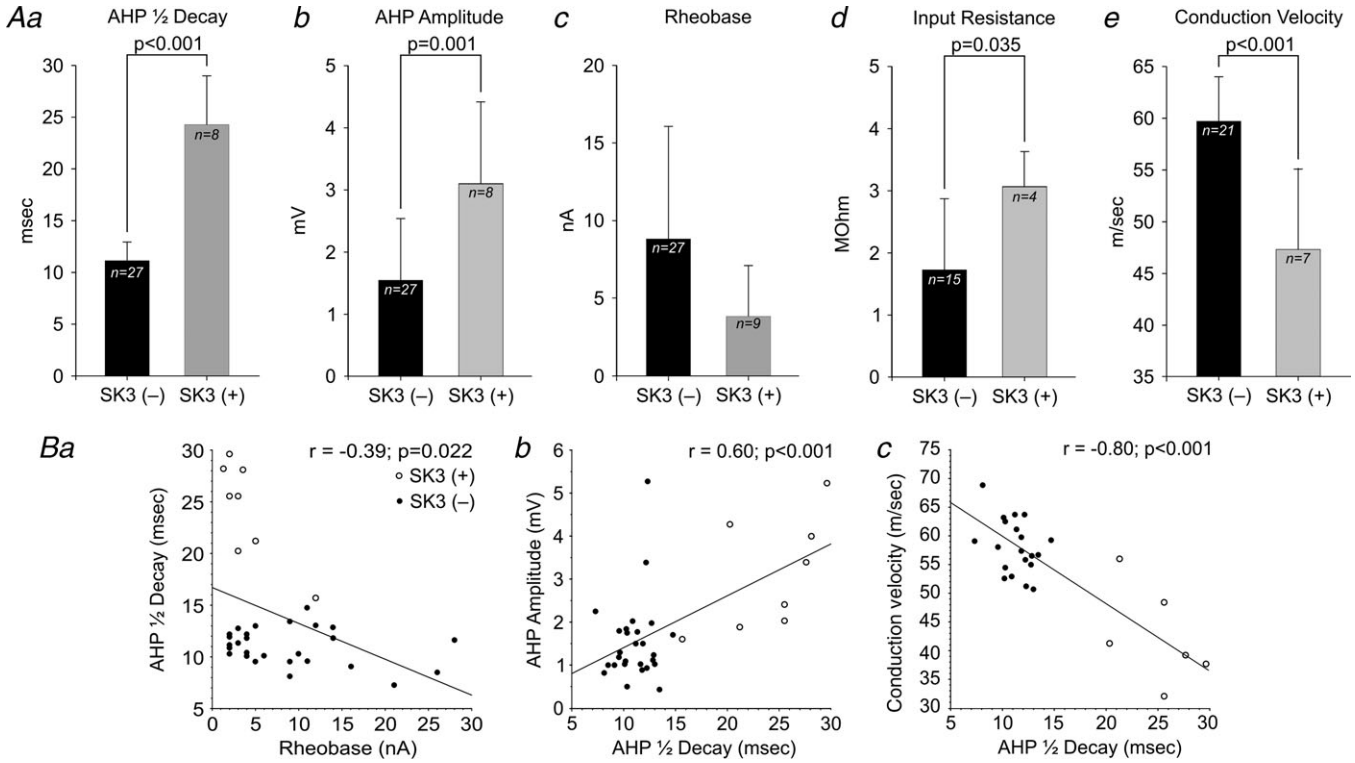

Figure 7. Electrical properties in SK3(+) and SK3(−) tibial motoneurons
A, average MN properties in SK3(+) and SK3(−) cells expressed as means ± SD. The SK3(+) cells have a significantly longer AHP half-decay time (*Aa*, 24.2 ± 4.7 *vs.* 11.0 ± 1.8 ms; Student's unpaired *t* test, $P < 0.001$), significantly greater AHP amplitude (*Ab*, 3.1 ± 1.3 *vs.* 1.5 ± 1.0 mV, Student's unpaired *t* test, $P = 0.001$), significantly greater input resistance (*Ad*, 3.1 ± 0.5 *vs.* 1.7 ± 1.1 Mω, Student's unpaired *t* test, $P = 0.035$) and significantly slower axonal conduction velocity (*Ae*, 44.2 ± 9.1 *vs.* 58.6 ± 5.1 m s^{-1}; Student's unpaired *t* test, $P < 0.001$) than SK3(−) cells. Although there was no significant difference in rheobase between SK3(+) and SK3(−) cells in the present sample (*Ac*, 3.8 ± 3.3 *vs.* 8.8 ± 7.3 nA, Student's unpaired *t* test, $P = 0.55$), there was a trend towards SK3(+) cells having much lower rheobase. *B*, covariance of AHP half-decay time with neuronal electrical properties (see also Eccles *et al.* 1958; Bakels & Kernell, 1993; Prather *et al.* 2011). Open circles indicate SK3(+) cells. Filled circles represent SK3(−) cells. All linear regression correlation coefficients (r) were significant (Pearson correlation, $P < 0.05$) and represent all MNs analysed, regardless of SK3 expression. *Ba*, AHP half-decay plotted *vs.* rheobase shows a weak but significant negative correlation ($r = -0.39$; $P = 0.022$). It is important to note that SK3(+) cells (open circles) cluster in the low-rheobase, long-AHP half-decay time region of the graph. Another group of low-rheobase cells is apparent, which have short AHPs and lack SK3-IR; the electrical properties of these cells fit previously described distributions, confirming that the relationship between AHP and rheobase is complex. *Bb*, AHP amplitude plotted *vs.* AHP half-decay shows a weak but positive correlation ($r = 0.60$; $P < 0.001$). *Bc*, axonal conduction velocity plotted *vs.* AHP half-decay shows a strong and significant negative correlation ($r = -0.80$; $P < 0.001$). In this plot, SK3(+) and SK3(−) cells separate into distinct clusters, with SK3(+) cells being found in the slow conduction velocity and long AHP half-decay region of the graph typical of S-type MNs. Corresponding conduction velocity and AHP measurements are unavailable for six SK3(−) and two SK3(+) cells, including the SK3(+) cell with the shortest AHP half-decay time.

© 2012 The Authors. The Journal of Physiology © 2012 The Physiological Society

2004). The precise colocalization between SK3-IR and Kv2.1-IR in these large cluster domains was consistent in all 341 clusters examined in 30 MNs. Note that small Kv2.1 clusters distributed widely across the surface membrane (Fig. 12*Ab*), independent of the large clusters, did not colocalize with SK-IR. This is consistent with the fact that Kv2.1 channel clusters are present in addition at non-cholinergic synapses on MNs and that these latter clusters are much smaller than the Kv2.1 clusters localized at C-bouton inputs (Muennich & Fyffe, 2004).

Discussion

Certain intrinsic membrane properties of spinal α-MNs vary systematically in relationship to motor unit type. It is well established that MNs of S-type motor units have larger amplitude and longer duration AHPs than do F-type MNs (Burke, 1967; Zengel *et al.* 1985; Gardiner, 1993). In α-MNs, as in other central neurons, the AHP displays multiple phases (fast, medium and slow AHP) that can be identified by their kinetics and pharmacological sensitivity to channel blockers (Schwindt *et al.* 1992; Viana *et al.* 1993; Sawczuk *et al.* 1997; Sah & Faber, 2002; Bond *et al.* 2004; Villalobos *et al.* 2004; Faber, 2009), although the slow AHP is rarely observed in MNs. There has been extensive effort to define the molecular identities, modulation and properties of the Ca^{2+}-activated K^+ channels that underlie kinetically different AHP currents in a variety of central neurons (Sah & Faber, 2002). These analyses suggest that large-conductance (BK) channels, in addition to TEA-sensitive voltage-gated K^+ channels, contribute to spike repolarization and to the fast AHP, whilst small-conductance Ca^{2+}-activated potassium (SK) channels, which have activation kinetics of several milliseconds and decay time constants of tens of milliseconds, contribute in large part to the mAHP (Viana *et al.* 1993; McLarnon, 1995; Sah & Faber 2002). The identity of the apamin-insensitive channels that underlie slow AHPs has not yet been confirmed (Sah & Faber, 2002; Bond *et al.* 2004; Power & Sah, 2008). Given the major physiological role of SK channels in the generation of mAHPs, hence MN firing properties, part of the motivation for the present study was to determine whether expression of particular SK channel isoforms might be correlated with the kinetically different mAHPs produced in different functional classes of MNs.

Another impetus for the present study was the notion that compartmentalized localization of SK channels

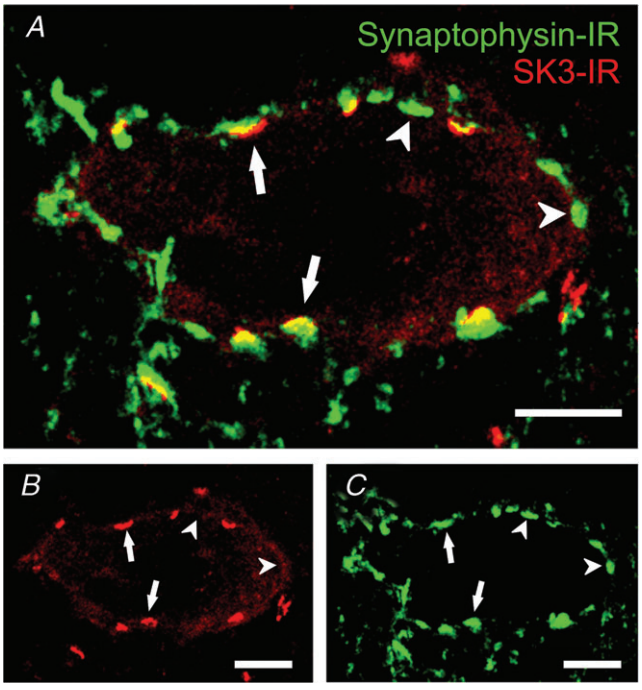

Figure 8. SK channel clusters are localized to synapses on α-motoneurons
A, arrows indicate some of the close appositions of boutons labelled with the presynaptic marker synaptophysin (green) and corresponding patches of postsynaptic SK3-IR (red; rat MN, three optical sections at 1.0 μm Z-steps). Some synaptophysin-IR boutons (arrowheads) do not appear to have any associated SK3-IR. The SK3-IR appears to be highly associated with the largest presynaptic boutons on α-MNs. *B*, SK3-IR only. *C*, synaptophysin-IR only. Scale bars represent 10 μm.

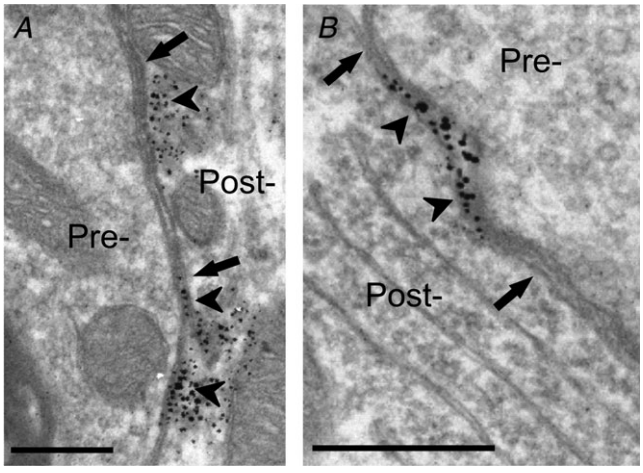

Figure 9. SK channels are localized to postsynaptic membrane sites at large C-bouton synapses on α-motoneurons
Ultrastructural analysis at synapses formed by presynaptic C-boutons (Pre-) shows SK3-IR labelling (arrowheads) localized to the membrane region of the postsynaptic α-MN (Post-). The synapses are characterized by the large size of the spherical synaptic vesicle-containing presynaptic boutons and by the presence of a postsynaptic subsurface cistern (arrows). *A*, SK3-IR at a C-bouton contact on a proximal dendrite. In this example, the presence of cytoplasmic labelling immediately beneath the postsynaptic membrane may represent channel protein being trafficked to or from the membrane, as described for Kv2.1 channels (Muennich & Fyffe, 2004). *B*, SK3-IR at a C-bouton contact on the MN soma. Scale bars represent 0.5 μm.

© 2012 The Authors. The Journal of Physiology © 2012 The Physiological Society

could be important for their physiological roles. In other regions of the brain, SK channels are localized at excitatory, glutamatergic synapses located on dendritic spines of hippocampal pyramidal neurons and neurons of the lateral amygdala (Faber *et al.* 2005, 2008; Lin *et al.* 2008). In the dendritic spines of these neurons, SK channels, especially SK2, appear to contribute to aspects of synaptic plasticity (Faber *et al.* 2005; Power

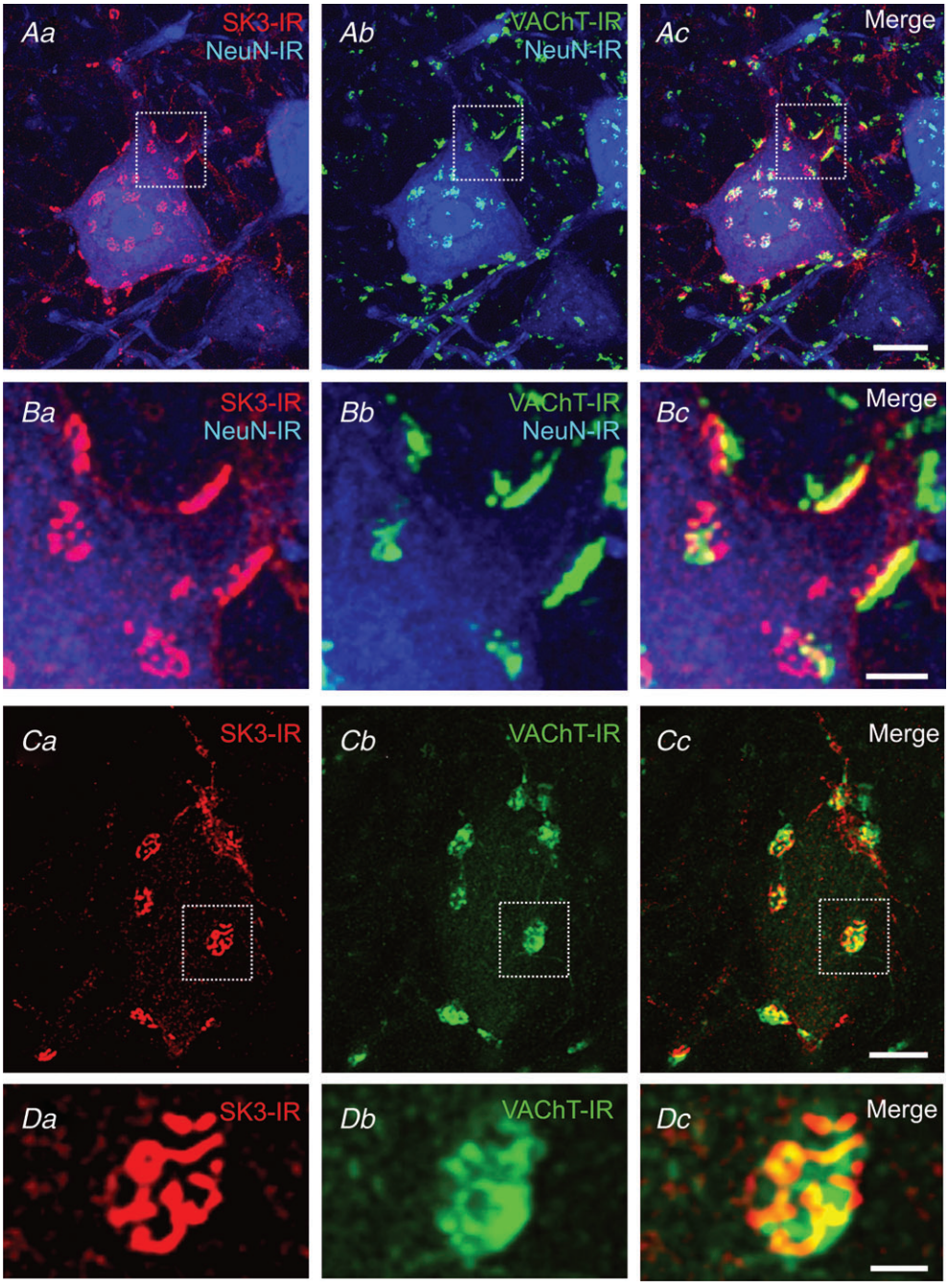

Figure 10. SK channels are clustered postsynaptically at cholinergic C-bouton synapses
Confocal images (stacks from 1 μm optical sections) of SK3-IR (red), NeuN-IR (blue) and vesicular acetylcholine transporter (VAChT)-IR (green) on rat lumbar α-MNs. The areas outlined in *Aa*–*c* (23 optical sections; scale bar represents 20 μm) are presented at higher magnification in *Ba*–*c* (23 optical sections; scale bar represents 5 μm), respectively, to show close apposition, 'edge on', of large cholinergic (VAChT-IR) boutons and clusters of postsynaptic SK3-IR. *Ca*–*c* (scale bar represents 10 μm), shown at higher magnification in *Da*–*c* (three optical sections; scale bar represents 2.5 μm) show '*en face*' SK3 clusters, with one of them (boxed area in *Ca*–*c*) being overlain by a cholinergic presynaptic bouton (*Cc* and *Dc*).

© 2012 The Authors. The Journal of Physiology © 2012 The Physiological Society

& Sah, 2008). These and related studies have also revealed that the activity and membrane trafficking of SK channels, as well as their calcium sensitivity, can be regulated by NMDA receptor activation and by a variety of neuromodulators, including those acting via muscarinic receptors and β-adrenoceptors, that affect calcium signalling or activation of kinases (Faber *et al.* 2008; Maingret *et al.* 2008; Faber, 2009). Given that spinal α-MNs essentially lack dendritic spines (Brown & Fyffe, 1981), it is of major interest to determine how SK channels are distributed, if at all, along spine-free dendrites, and if they are associated with excitatory synapses as they are in other neurons.

The general expression profile of SK channels in the CNS has been revealed using *in situ* hybridization and immunostaining against SK channel protein or myc-tagged epitopes, and the main subunit types are widely expressed in partly overlapping distributions (Stocker & Pedarzani, 2000; Tacconi *et al.* 2001; Sailer *et al.* 2004). The present study demonstrates that α-MNs in cat, rat and mouse lumbar spinal cord express specific members of the SK channel family, in accordance with observations that the mAHP in these neurons (and in hypoglossal MNs) is blocked by apamin (Zhang & Krnjević, 1987; Hounsgaard *et al.* 1988; Viana *et al.* 1993; Sawczuk *et al.* 1997; Powers *et al.* 1999; Miles *et al.* 2005). Several novel and unexpected features of SK channel expression and distribution in spinal MNs are revealed by detailed analysis of channel localization. First, we reveal in rats and mice a differential expression of specific SK subunits (SK2 *vs.* SK3) among differently sized α-MNs with different electrophysiological properties. Second, SK2 and SK3 channels in the aspinous surface membrane of α-MNs are organized in a highly clustered

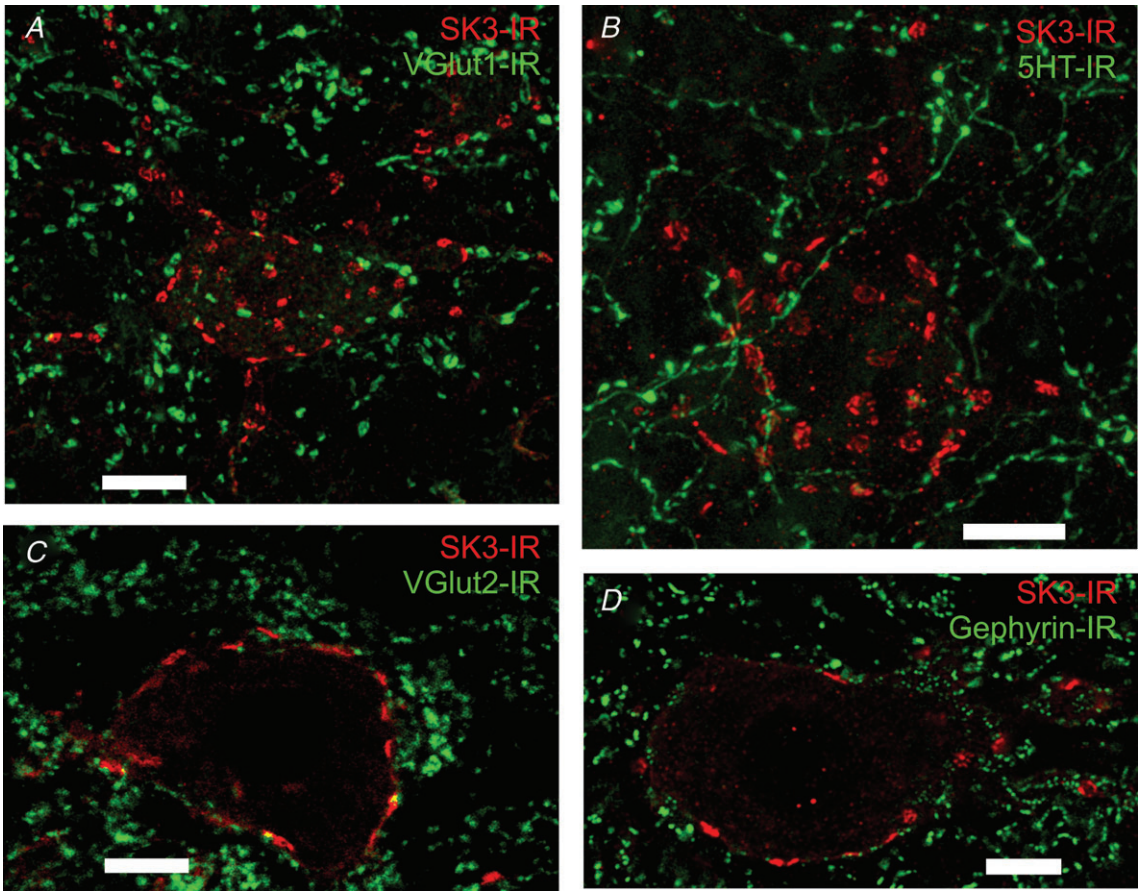

Figure 11. SK channels do not colocalize with glutamatergic, serotonergic and inhibitory synapses
Images are representative high-power (×60 objective) rodent lumbar α-MNs. *A*, confocal image stack (21 optical sections at 1.0 μm Z-steps) shows no observable association with VGLUT1-IR (green), which labels a specific population of glutamatergic synapses, and SK3-IR (red). Scale bar represents 20.0 μm *B*, confocal image stack (32 optical sections at 1.0 μm Z-steps) shows no observable association with 5HT-IR (green), which labels serotonergic synapses, and SK3-IR (red). Scale bar represents 10.0 μm. *C*, confocal single optical section shows no observable association with VGLUT2-IR (green), which labels a specific population of glutamatergic synapses, and SK3-IR (red). Scale bar represents 10.0 μm. *D*, single optical confocal section shows no observable association with gephyrin-IR (green), which labels GABAergic and glycinergic synapses, and SK3-IR (red). Scale bar represents 10.0 μm.

© 2012 The Authors. The Journal of Physiology © 2012 The Physiological Society

pattern and are restricted to the soma and proximal dendrites. Third, SK channels are selectively localized at postsynaptic sites associated with cholinergic C-boutons and are thus colocalized with Kv2.1 channels and m_2 muscarinic receptors at these sites. Interestingly, new evidence has indicated that state-dependent m_2 receptor activation by cholinergic C-boutons increases motoneuron excitability by reducing action potential AHP (Miles *et al.* 2007; Zagoraiou *et al.* 2009); however, a mechanism of interaction between m_2 receptors and SK channels has yet to be defined.

SK2 and SK3 channels are expressed in different populations of MNs in rats and mice but not in cats

In this study, MNs were identified by anatomical parameters (e.g. soma size/morphology and location within lamina IX) as well as by molecular markers (e.g. VAChT and NeuN immunoreactivity) that allowed us to differentiate α-MNs from γ-MNs and interneurons (Moschovakis *et al.* 1991; Alvarez & Fyffe, 2007; Friese *et al.* 2009; Shneider *et al.* 2009). All MN soma measurements fell within the range of soma diameters previously described for α-MNs (Chen & Wolpaw, 1994; Ishihara *et al.* 2001; Bose *et al.* 2005). Through use of the common neuronal marker, NeuN, our analyses revealed an unexpected relationship between the level of expression of NeuN and MN soma size. Neurons that expressed high levels of NeuN in the nucleus and cytoplasm were, on average, larger than neurons that expressed low levels of NeuN in the cytoplasm. Other recent reports suggest that γ-MNs lack expression of NeuN (Friese *et al.* 2009; Shneider *et al.* 2009) as do cerebellar Purkinje cells, mitral cells of the olfactory bulb, inferior olivary neurons, basket

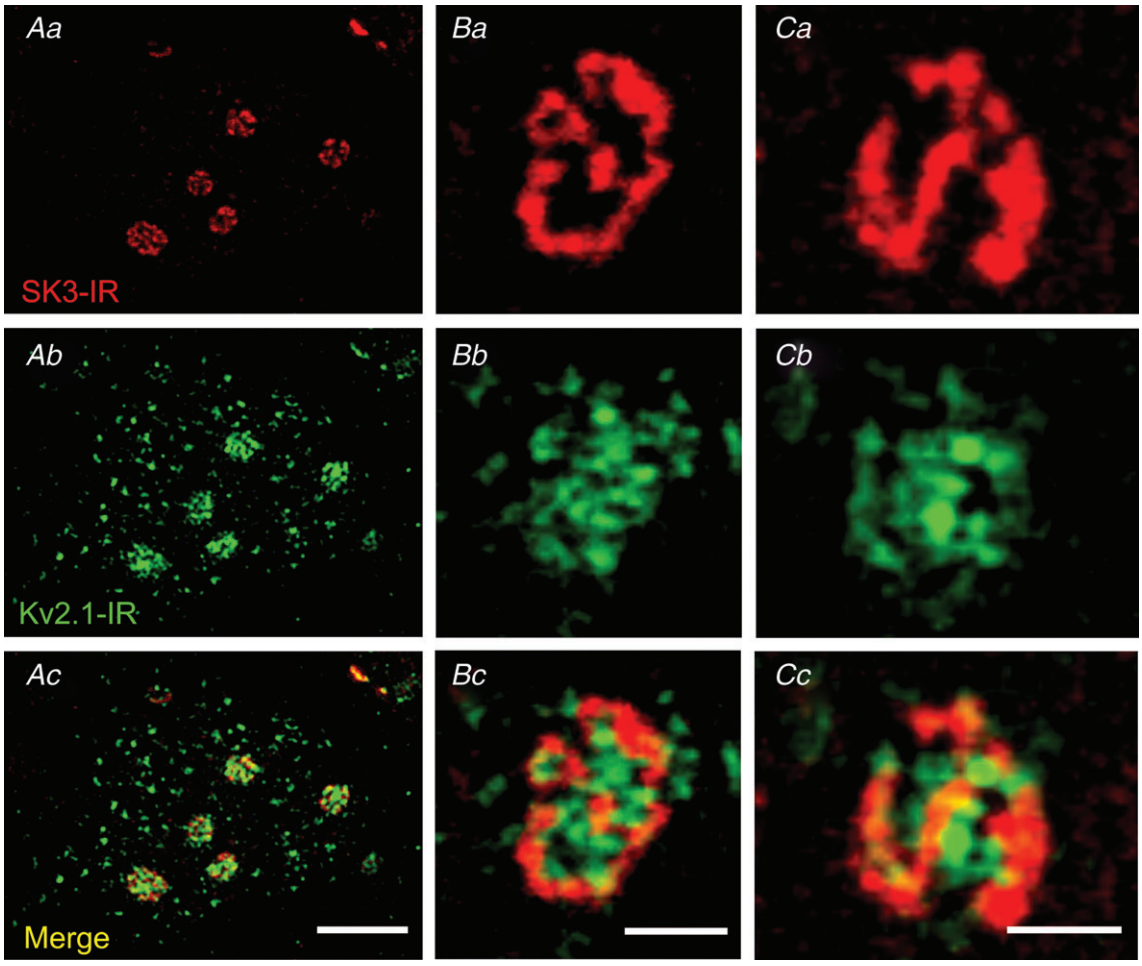

Figure 12. SK channel clusters are colocalized postsynaptically with large Kv2.1-IR clusters
Images are representative micrographs from small confocal microscopy stacks of SK3-IR (red) and Kv2.1 (green) *A*, small high-power confocal stack (×60 objective) of rat α-MN membrane, showing that SK3-IR is not present at all Kv2.1 clusters but is present at the largest Kv2.1 clusters. Confocal image stack is three optical sections (1.0 μm Z-step). Scale bar represents 10 μm. *B* and *C*, representative examples of *en face* SK3-IR and Kv2.1-IR clusters. Within the clusters, Kv2.1-IR tends to be more diffuse, while SK3-IR tends to be fenestrated. Confocal image stacks are two optical sections (1.0 μm Z-step). Scale bars represent 2 μm.

© 2012 The Authors. The Journal of Physiology © 2012 The Physiological Society

and stellate interneurons of the cerebellum, and retinal photoreceptors (Mullen *et al.* 1992; Wolf *et al.* 1996; Sarnat *et al.* 1998; Weyer & Schilling, 2003). Such observations of non-uniform expression of NeuN emphasize the need for caution when using NeuN as a presumed ubiquitous neuronal marker in spinal cord, particularly given that its level of expression may also be modulated by injury (McPhail *et al.* 2004; Alvarez *et al.* 2011).

Two α-MN populations were distinguished in rats and mice by virtue of their differential expression of SK2 *vs.* SK3 channel isoforms. All MNs express SK2, and a minority of MNs are distinguished by expression of SK3 plus SK2; the majority of MNs express only SK2. The SK2-IR MNs outnumber SK3-IR/SK2-IR MNs in a ratio consistent with the overall ratio of F-type to S-type motoneurons in most lumbosacral MN pools. Importantly, the expression of SK2 *vs.* SK3/SK2 was correlated with α-MN soma size of the respective populations. The predominant membrane SK channel in small α-MNs is SK3, with these neurons also displaying SK2-IR. Conversely, large α-MNs have prominent membrane expression of SK2 but lack SK3. Consistent with the substantial evidence that MN size varies by motor unit type in the order S < F (Burke *et al.* 1982; Cullheim *et al.* 1987), a significantly greater proportion of soleus MNs (predominantly slow-twitch) express SK3 than gastrocnemius MNs (predominantly fast-twitch), indicating that SK3 subunits are preferentially expressed in S-type rat MNs. The observation that the medial motor pools, which innervate slow-twitch postural muscles, also contain a high level of SK3-IR in mice and rats further supports MN type-specific SK3 expression in rodent MNs. In cats, all MNs, i.e. both S- and F-types, appear to express SK3. Although the implications of this interspecies difference remain to be determined, it is of interest that the AHPs in cat MNs, even F-types, tend to be larger and longer than the AHPs observed in rat and mouse MNs.

Motoneuron electrophysiological properties in this study fell within the range of measurements previously described for rat α-MNs (Bakels & Kernell, 1993; Seburn & Cope, 1998; Bichler *et al.* 2007*a*,*b*; Bullinger *et al.* 2011). Our electrophysiological analyses revealed a significantly longer duration and larger amplitude AHP in rat MNs expressing SK3. Importantly, Gardiner (1993) reports distinguishing fast from slow motoneurons in the rat medial gastrocnemius motor pool with 100% accuracy using a single parameter, namely a nominal cut-off between F- and S-types of 20 ms AHP half-decay time (F-type AHP half-decay < 19 ms; and S-type AHP half-decay > 20 ms). In the present study, seven of the eight physiologically characterized, SK3-expressing MNs had AHP half-decay times greater than 20 ms and would probably be S-type based on Gardiner's criteria. The data of Bakels & Kernell (1993) show several S-type MNs with AHP half-decay shorter than 15 ms (their average was 18.3 ± 6.3 ms), indicating that all eight SK3-IR cells in our study fall within the range of AHP durations previously observed in S-type MNs. The variation among reported electrophysiological parameters from the few *in vivo* reports that are available underscores, as mentioned by Bakels & Kernell (1993), that physiological properties of motor units display continuous variation in magnitude and that classification into categories, such as 'fast' or 'slow,' is still controversial (Mendell, 2005) and often made for convenience in description, analysis and comparative study. Despite this caveat, our data appear to correlate well with the data of Gardiner (1993), and our interpretation is strengthened by further correlation with other electrophysiological properties.

While other molecular factors have been postulated to distinguish S- and F-type MNs (Forsgren *et al.* 1993; Piehl *et al.* 1993; Chakkalakal *et al.* 2010; Enjin *et al.* 2010), to date there are no indications in the literature of specific ion channels that might underlie physiological differences between S- and F-type MNs. The present results suggest that differential expression of SK isoforms contributes to the observed variability in rat motoneuron mAHP duration and, in particular, that the presence of SK3 channel subunits is associated with long-duration mAHP currents in small, presumably S-type, rat MNs. The finding that SK3-expressing MNs in this study share other known physiological properties predictive of S-type MNs, such as slower conduction velocity and a trend towards lower rheobase (differences in rheobase did not reach significance, probably due to our intentional sampling bias; see also Gardiner, 1993), strongly suggests that SK3-IR may serve as an anatomical marker for rodent S-type MNs. However, caution must be taken in interpreting motor unit classification of SK3-expressing MNs without corresponding twitch data from innervated muscle fibres, and in cases where motoneuron axons have been subjected to injury (unpublished observations from AS Deardorff, SH Romer, and REW Fyffe).

Furthermore, the fact that all cat MNs express SK3 subunits obviously complicates any attempt to correlate systematically a specific SK channel isoform with the distinct mAHP time courses of different types of MNs across species. One speculative explanation to reconcile the interspecies differences is to consider the 'absolute' mAHP duration rather than the relative differences across S- or F-type MNs in a single species. We plotted (not shown) mean values and ranges from the literature of AHP half-decay time for cat and rat F- and S-type MNs and for mouse MNs (for which there are no type-specific data), which showed the predictable trend for cat S-type > cat F-type > rat S-type > rat F-type > mouse. However, the ranges overlap extensively, particularly between rat F-type, rat S-type and mouse data, and between rat S-type and cat F-type. Gardiner & Kernell (1990) also showed that the

© 2012 The Authors. The Journal of Physiology © 2012 The Physiological Society

longest duration AHPs in rat S-type MNs are at least as long as many of the AHPs in cat F-type MNs. Our data suggest that expression of SK2 only, i.e. lack of SK3, is associated with the shortest AHPs in absolute terms, i.e. those in large F-type MNs in rat and mouse. Conversely, SK3 appears to be present in MNs with longer duration AHPs in absolute terms, namely small S-type MNs in rats and mice and all MNs in cats. Given that, in general, the relative contractile speed of muscle fibres in the three species analysed increases in the order cat < rat < mice, it is likely that rodent F-type motoneurons lack SK3 in order for them to fire at rates necessary to match the contractile speed of their innervated muscle fibres effectively. We believe that extrapolation of this conclusion is merited, despite the absence of type specification for measured AHP values in the mouse, because the longest mouse AHPs, presumably from S-type MNs, have durations that overlap with those of rat S-type MNs. Although the molecular mechanisms that may underlie these observed differences in mAHP duration are not yet defined, this conclusion is further supported by findings that SK3 channels have slower activation and deactivation time constants than SK2 channels (Xia *et al.* 1998). Moreover, SK3 expression may only be one factor underlying the observed variability in AHP duration in rat MNs, and other factors, such as differential coupling of SK channels to Ca^{2+} sources, variations in SK channel cluster sizes/density, the presence/absence of hyperpolarization-activated currents (Ih) and/or synaptic modulation of AHP kinetics, may need to be considered.

There is another level of uncertainty in any attempt to ascribe AHP kinetics to specific SK contributions, because we lack information on the third isoform, SK1, for which, unfortunately there is no reliable antibody available for specific detection or localization. Rat SK1, transfected and expressed alone in HEK 293 cells, was unable to produce a Ca^{2+}-activated K^+ conductance (Benton *et al.* 2003). However, when SK1 and SK2 were coexpressed, there was a Ca^{2+}-activated K^+ conductance that was larger in magnitude, with decreased apamin sensitivity, than when SK2 was expressed alone (Benton *et al.* 2003). It is now known that rat SK1 subunits can form heteromeric channels with rat SK2 but not SK3 (Benton *et al.* 2003; Monaghan *et al.* 2004; Strassmaier *et al.* 2005). Furthermore, SK3 can form heteromeric subunits only with SK2, suggesting SK1 may play a role in disrupting SK3 assemblies (Monaghan *et al.* 2004). Thus, even in rodent MNs where SK2 and SK3 exhibit differential expression patterns, SK1 could potentially be present and modify channel characteristics. Therefore, we must at present conclude that the well-documented and varying AHP properties of S- and F-type MNs cannot be ascribed simply to SK2 *vs.* SK3 expression but may reflect specific patterns of SK1 expression, heteromeric combinations of multiple SK isoforms, or contributions from different regulatory mechanisms or ion conductances (for example, AHP duration in cat MNs varies inversely with the magnitude of their sag current; Gustafsson & Pinter, 1985). Thus, complete understanding of the contribution of specific SK subunits to AHP properties awaits the following findings: (i) clear molecular evidence of the presence or absence of SK1 in MNs; (ii) further determination, possibly in expression systems, of the functional properties of heteromeric SK channels; and (iii) examination of other intrinsic/extrinsic mechanisms that may contribute to AHP variability.

Membrane organization of SK channels

A novel and important finding of this study is that SK2 and SK3 channels are selectively localized at postsynaptic sites on the soma and proximal dendrites of MNs. Both confocal microscopy and ultrastructural analyses confirm that SK channel expression is enriched, particularly in large clusters immediately adjacent to cholinergic C-boutons, in a manner reminiscent of Kv2.1 channel distribution (Muennich & Fyffe, 2004).

Muscarinic m_2 receptors are the dominant muscarinic acetylcholine receptor subtype in the MN plasma membrane and, like SK and Kv2.1 channels, localize directly adjacent to C-boutons (Skinner *et al.* 1999; Hellström *et al.* 2003; Muennich & Fyffe, 2004). Muscarinic acetylcholine receptors can be classified into five subtypes ($m_1 - m_5$), which transduce signals through distinct G-protein-coupled pathways. Recent evidence indicates that m_2 receptor activation by cholinergic C-boutons during fictive locomotion increases spinal MN excitability by reducing the AHP (Miles *et al.* 2007; Zagoraiou *et al.* 2009). Similar reductions in AHP have been observed following muscarinic receptor activation of hypoglossal MNs (Lape & Nistri, 2000). The distinct subcellular localization of SK channels correlates well with these physiological data and suggests that reduced outward SK current following cholinergic m_2 receptor stimulation may mediate this reduction in AHP.

While muscarinic acetylcholine receptors can evoke cellular effects through a variety of signalling cascades (Shapiro *et al.* 1999; Hoshi *et al.* 2003; Tiran *et al.* 2003; Zhou *et al.* 2003), m_2 receptors typically couple to pertussis toxin-sensitive G_i/G_o pathways which, when activated, can reduce adenylate cyclase or directly inhibit voltage-gated Ca^{2+} channels (Hille, 1994; Stewart *et al.* 1999; Santafé *et al.* 2006). Membrane delimited pertussis toxin-sensitive muscarinic blockade of N- and P/Q-type Ca^{2+} currents have been observed in a variety of cell types (Allen & Brown, 1993; Hille, 1994; Howe & Surmeier, 1995; Stewart *et al.* 1999; Santafé *et al.* 2006). Blockade is usually caused by m_2-coupled, $\beta\gamma$-mediated, depolarizing shifts in the voltage dependence of channel activation and is transiently relieved by strong or repeated depolarization

© 2012 The Authors. The Journal of Physiology © 2012 The Physiological Society

(Hille, 1994; Ikeda, 1996; Jeong *et al.* 1999; Shapiro *et al.* 1999; Herlitze & Landmesser, 2007). Interestingly, in hypoglossal and spinal MNs, conotoxin-sensitive N- and P/Q-type Ca^{2+} currents provide the calcium for SK channel activation (Viana *et al.* 1993; Bayliss *et al.* 1995; Li & Bennett, 2007); therefore, C-bouton-mediated reductions in MN AHP may occur via $\beta\gamma$ inhibition of N- and P/Q-type Ca^{2+} currents in the vicinity of SK channels. Such a role for MN m_2 receptors is intriguing in light of findings that Ca^{2+}-dependent modulation of Kv2.1 channel gating increases outward K^+ current and reduces neuronal firing rate (Misonou *et al.* 2004; Mohapatra *et al.*, 2009; Surmeier & Foehring, 2004). It is possible that m_2 receptor activation serves to regulate outward current through SK and Kv2.1 channels via an intermediary effect on local $[Ca^{2+}]_i$, and thereby provide state-dependent modulation of MN firing rate. However, despite ample evidence for muscarine-evoked, m_2 receptor-mediated reduction of neuronal N- and P/Q-type Ca^{2+} channels, Miles *et al.* (2007) were unable to elicit MN Ca^{2+} current modulation following bath application of muscarine in whole-cell voltage-clamp experiments. This result underscores the necessity for anatomical characterization of MN voltage-gated Ca^{2+} channels, because it is difficult to interpret pharmacological manipulation of global Ca^{2+} currents without knowledge of the subcellular localization of specific channel subtypes. It is possible that conotoxin-sensitive Ca^{2+} channels in the vicinity of MN m_2 receptors represent only a minority of MN somatic Ca^{2+} sources, and their blockade may be masked in studies of global Ca^{2+} currents by other, extrasynaptic Ca^{2+} channels.

Alternatively, the direct phosphorylation of SK channels by protein kinase A and casein kinase 2 can cause channel internalization (Kohler *et al.* 1996; Ren *et al.* 2006; Faber *et al.* 2008; Lin *et al.* 2008) and reduced Ca^{2+} sensitivity (Allen *et al.* 2007), respectively. Although m_2 receptors typically inhibit protein kinase activity, other phosphorylation pathways may be activated by m_2 receptors (Zhou *et al.* 2003), and it is possible that muscarinic reductions in AHP occur via direct phosphorylation of SK channels. A corollary of this is that Kv2.1 is also highly regulated by phosphorylation (Misonou *et al.* 2004), and the strategic localization of Kv2.1 clusters may suggest the presence of a currently undefined neuronal m_2 receptor-mediated phosphorylation pathway.

It should be noted that recent electrophysiological evidence has indicated the presence of a separate population of dendritic SK channels activated by persistent inward Ca^{2+} currents that are spatially distinct from SK channels responsible for generating the AHP (Li & Bennett, 2007). The $Ca_v1.3$ (L-type) channels mediating persistent inward Ca^{2+} currents are found in MN dendrites (Carlin *et al.* 2000). Subsequent studies have predicted these channels to localize in dendritic hot spots occurring at least 100 μm away from the soma (Elbasiouny *et al.* 2005; Bui *et al.* 2006). In the present study, however, dendritic SK-IR was observed only in large clusters apposed to C-bouton synapses within the initial 150–200 μm of the dendritic tree. When intracellularly labelled MN dendrites were carefully examined, we did not observe synaptic or extrasynaptic SK expression beyond the first 200 μm length of dendritic membrane. Nevertheless, we observed a significant amount of punctate SK-IR, apparently associated with dendritic profiles throughout laminae VII and IX, but could not identify the source of this labelling. It should be noted that the expression of SK1 remains undefined, but even if SK1 is present extrasynaptically in dendrites, it probably requires SK2 to construct functional heteromeric assemblies (e.g. Benton *et al.* 2003). Thus, while it is possible that the dendritic SK conductances proposed by Li & Bennett (2007) represent functional homomeric SK1 channels, it is also possible that the the density of extrasynaptic SK2 (or SK3) channels in the proximal and distal dendrites we have been able to analyse in detail is below the threshold for detection by our methods.

Conclusions

In summary, the present shows the following results: (i) there is a differential expression of SK3-IR in rodent, but not cat, motoneurons; (ii) rat α-MNs expressing SK3-IR are significantly smaller, have a significantly slower axon conduction velocity and have a significantly longer AHP half-decay time and larger AHP amplitude and than α-MNs not expressing SK3-IR; (iii) rat MN pools innervating slow-twitch muscles have a higher percentage of SK3-IR α-MNs than those innervating fast-twitch muscles; and (iv) SK2 and SK3 channel clusters appose cholinergic C-boutons. These data suggest that the presence of SK3 subunits may be a molecular factor differentiating between S- and F-type MNs. Furthermore, the specific clustering and synaptic localization of SK2 and SK3 together with m_2 receptors and Kv2.1 channels is likely to represent a novel cellular mechanism for the state-dependent regulation of neuronal excitability.

References

Allen D, Fakler B, Maylie J & Adelman JP (2007). Organization and regulation of small conductance Ca^{2+}-activated K^+ channel multiprotein complexes. *J Neurosci* **27**, 2369–2376.

Allen TG & Brown DA (1993). M_2 muscarinic receptor-mediated inhibition of the Ca^{2+} current in rat magnocellular cholinergic basal forebrain neurones. *J Physiol* **466**, 173–189.

Alvarez FJ, Dewey DE, Harrington DA & Fyffe RE (1997). Cell-type specific organization of glycine receptor clusters in the mammalian spinal cord. *J Comp Neurol* **379**, 150–170.

© 2012 The Authors. The Journal of Physiology © 2012 The Physiological Society

Alvarez FJ, Dewey DE, McMillin P & Fyffe RE (1999). Distribution of cholinergic contacts on Renshaw cells in the rat spinal cord: a light microscopic study. *J Physiol* **515**, 787–797.

Alvarez FJ & Fyffe RE (2007). The continuing case for the Renshaw cell. *J Physiol* **584**, 31–45.

Alvarez FJ, Pearson JC, Harrington D, Dewey D, Torbeck L & Fyffe RE (1998). Distribution of 5-hydroxytryptamine-immunoreactive boutons on α-motoneurons in the lumbar spinal cord of adult cats. *J Comp Neurol* **393**, 69–83.

Alvarez FJ, Titus-Mitchell HE, Bullinger KL, Kraszpulski M, Nardelli P & Cope TC (2011). Permanent central synaptic disconnection of proprioceptors after nerve injury and regeneration. I. Loss of VGLUT1/IA synapses on motoneurons. *J Neurophysiol* **106**, 2450–2470.

Alvarez FJ, Villalba RM, Zerda R & Schneider SP (2004). Vesicular glutamate transporters in the spinal cord, with special reference to sensory primary afferent synapses. *J Comp Neurol* **472**, 257–280.

Armstrong WE, Rubrum A, Teruyama R, Bond CT & Adelman JP (2005). Immunocytochemical localization of small-conductance, calcium-dependent potassium channels in astrocytes of the rat supraoptic nucleus. *J Comp Neurol* **491**, 175–185.

Bakels R & Kernell D (1993). Matching between motoneurone and muscle unit properties in rat medial gastrocnemius. *J Physiol* **463**, 307–324.

Baldissera F & Gustafsson B (1974). Firing behaviour of a neurone model based on the afterhyperpolarization conductance time course and algebraical summation. Adaptation and steady state firing. *Acta Physiol Scand* **92**, 27–47.

Bayliss DA, Umemiya M & Berger AJ (1995). Inhibition of N- and P-type calcium currents and the after-hyperpolarization in rat motoneurones by serotonin. *J Physiol* **485**, 635–647.

Benton DC, Monaghan AS, Hosseini R, Bahia PK, Haylett DG & Moss GW (2003). Small conductance Ca^{2+}-activated K^+ channels formed by the expression of rat *SK1* and *SK2* genes in HEK 293 cells. *J Physiol* **553**, 13–19.

Bichler EK, Carrasco DI, Rich MM, Cope TC & Pinter MJ (2007*a*). Rat motoneuron properties recover following reinnervation in the absence of muscle activity and evoked acetylcholine release. *J Physiol* **585**, 47–56.

Bichler EK, Nakanishi ST, Wang QB, Pinter MJ, Rich MM & Cope TC (2007*b*). Enhanced transmission at a spinal synapse triggered *in vivo* by an injury signal independent of altered synaptic activity. *J Neurosci* **27**, 12851–12859.

Bond CT, Herson PS, Strassmaier T, Hammond R, Stackman R, Maylie J & Adelman JP (2004). Small conductance Ca^{2+}-activated K^+ channel knock-out mice reveal the identity of calcium-dependent afterhyperpolarization currents. *J Neurosci* **24**, 5301–5306.

Bose P, Parmer R, Reier PJ & Thompson FJ (2005). Morphological changes of the soleus motoneuron pool in chronic midthoracic contused rats. *Exp Neurol* **191**, 13–23.

Brown AG & Fyffe RE (1981). Direct observations on the contacts made between Ia afferent fibres and α-motoneurones in the cat's lumbosacral spinal cord. *J Physiol* **313**, 121–140.

Bui TV, Ter-Mikaelian M, Bedrossian D & Rose PK (2006). Computational estimation of the distribution of L-type Ca^{2+} channels in motoneurons based on variable threshold of activation of persistent inward currents. *J Neurophysiol* **95**, 225–241.

Bullinger KL, Nardelli P, Pinter MJ, Alvarez FJ & Cope TC (2011). Permanent central synaptic disconnection of proprioceptors after nerve injury and regeneration. II. Loss of functional connectivity with motoneurons. *J Neurophysiol* **106**, 2471–2485.

Burke RE (1967). Motor unit types of cat triceps surae muscle. *J Physiol* **193**, 141–160.

Burke RE, Dum RP, Fleshman JW, Glenn LL, Lev-Tov A, O'Donovan MJ & Pinter MJ (1982). A HRP study of the relation between cell size and motor unit type in cat ankle extensor motoneurons. *J Comp Neurol* **209**, 17–28.

Carlin KP, Jones KE, Jiang Z, Jordan LM & Brownstone RM (2000). Dendritic L-type calcium currents in mouse spinal motoneurons: implications for bistability. *Eur J Neurosci* **12**, 1635–1646.

Carr PA, Alvarez FJ, Leman EA & Fyffe RE (1998). Calbindin D28k expression in immunohistochemically identified Renshaw cells. *Neuroreport* **9**, 2657–2661.

Chakkalakal JV, Nishimune H, Ruas JL, Spiegelman BM & Sanes JR (2010). Retrograde influence of muscle fibers on their innervation revealed by a novel marker for slow motoneurons. *Development* **137**, 3489–3499.

Chen XY & Wolpaw JR (1994). Triceps surae motoneuron morphology in the rat: a quantitative light microscopic study. *J Comp Neurol* **343**, 143–157.

Conradi S, Kellerth JO & Berthold CH (1979). Electron microscopic studies of serially sectioned cat spinal alpha-motoneurons. II. A method for the description of architecture and synaptology of the cell body and proximal dendritic segments. *J Comp Neurol* **184**, 741–754.

Cullheim S, Fleshman JW, Glenn LL & Burke RE (1987). Membrane area and dendritic structure in type-identified triceps surae alpha motoneurons. *J Comp Neurol* **255**, 68–81.

Deng Z & Fyffe RE (2004). Expression of $P2X_7$ receptor immunoreactivity in distinct subsets of synaptic terminals in the ventral horn of rat lumbar spinal cord. *Brain Res* **1020**, 53–61.

Eccles JC, Eccles RM & Lundberg A (1957). Durations of after-hyperpolarization of motoneurones supplying fast and slow muscles. *Nature* **179**, 866–868.

Eccles JC, Eccles RM & Lundberg A (1958). The action potentials of the alpha motoneurones supplying fast and slow muscles. *J Physiol* **142**, 275–291.

Elbasiouny SM, Bennett DJ & Mushahwar VK (2005). Simulation of dendritic $Ca_V1.3$ channels in cat lumbar motoneurons: spatial distribution. *J Neurophysiol* **94**, 3961–3974.

Enjin A, Rabe N, Nakanishi ST, Vallstedt A, Gezelius H, Memic F, Lind M, Hjalt T, Tourtellotte WG, Bruder C, Eichele G, Whelan PJ & Kullander K (2010). Identification of novel spinal cholinergic genetic subtypes disclose *Chodl* and *Pitx2* as markers for fast motor neurons and partition cells. *J Comp Neurol* **518**, 2284–2304.

Faber ES (2009). Functions and modulation of neuronal SK channels. *Cell Biochem Biophys* **55**, 127–139.

© 2012 The Authors. The Journal of Physiology © 2012 The Physiological Society

Faber ES, Delaney AJ, Power JM, Sedlak PL, Crane JW & Sah P (2008). Modulation of SK channel trafficking by beta adrenoceptors enhances excitatory synaptic transmission and plasticity in the amygdala. *J Neurosci* **28**, 10803–10813.

Faber ES, Delaney AJ & Sah P (2005). SK channels regulate excitatory synaptic transmission and plasticity in the lateral amygdala. *Nat Neurosci* **8**, 635–641.

Faber ES & Sah P (2002). Physiological role of calcium-activated potassium currents in the rat lateral amygdala. *J Neurosci* **22**, 1618–1628.

Faber ES & Sah P (2003). Calcium-activated potassium channels: multiple contributions to neuronal function. *Neuroscientist* **9**, 181–194.

Forsgren S, Bergh A, Carlsson E & Thornell LE (1993). Calcitonin gene-related peptide expression at endplates of different fibre types in muscles in rat hind limbs. *Cell Tissue Res* **274**, 439–446.

Friese A, Kaltschmidt JA, Ladle DR, Sigrist M, Jessell TM & Arber S (2009). Gamma and alpha motor neurons distinguished by expression of transcription factor Err3. *Proc Natl Acad Sci U S A* **106**, 13588–13593.

Gardiner PF (1993). Physiological properties of motoneurons innervating different muscle unit types in rat gastrocnemius. *J Neurophysiol* **69**, 1160–1170.

Gardiner PF & Kernell D (1990). The "fastness" of rat motoneurones: time-course of afterhyperpolarization in relation to axonal conduction velocity and muscle unit contractile speed. *Pflugers Arch* **415**, 762–766.

Gustafsson B & Pinter MJ (1985). Factors determining the variation of the afterhyperpolarization duration in cat lumbar alpha-motoneurones. *Brain Res* **326**, 392–395.

Haftel VK, Bichler EK, Nichols TR, Pinter MJ & Cope TC (2004). Movement reduces the dynamic response of muscle spindle afferents and motoneuron synaptic potentials in rat. *J Neurophysiol* **91**, 2164–2171.

Haftel VK, Bichler EK, Wang QB, Prather JF, Pinter MJ & Cope TC (2005). Central suppression of regenerated proprioceptive afferents. *J Neurosci* **25**, 4733–4742.

Hellström J, Oliveira AL, Meister B & Cullheim S (2003). Large cholinergic nerve terminals on subsets of motoneurons and their relation to muscarinic receptor type 2. *J Comp Neurol* **460**, 476–486.

Henneman E & Olson CB (1965). Relations between structure and function in the design of skeletal muscles. *J Neurophysiol* **28**, 581–598.

Henneman E, Somjen G & Carpenter DO (1965*a*). Functional significance of cell size in spinal motoneurons. *J Neurophysiol* **28**, 560–580.

Henneman E, Somjen G & Carpenter DO (1965*b*). Excitability and inhibitability of motoneurons of different sizes. *J Neurophysiol* **28**, 599–620.

Herlitze S & Landmesser LT (2007). New optical tools for controlling neuronal activity. *Curr Opin Neurobiol* **17**, 87–94.

Hille B (1994). Modulation of ion-channel function by G-protein-coupled receptors. *Trends Neurosci* **17**, 531–536.

Hoshi N, Zhang JS, Omaki M, Takeuchi T, Yokoyama S, Wanaverbecq N, Langeberg LK, Yoneda Y, Scott JD, Brown DA & Higashida H (2003). AKAP150 signaling complex promotes suppression of the M-current by muscarinic agonists. *Nat Neurosci* **6**, 564–571.

Hounsgaard J, Kiehn O & Mintz I (1988). Response properties of motoneurones in a slice preparation of the turtle spinal cord. *J Physiol* **398**, 575–589.

Howe AR & Surmeier DJ (1995). Muscarinic receptors modulate N-, P-, and L-type Ca^{2+} currents in rat striatal neurons through parallel pathways. *J Neurosci* **15**, 458–469.

Ikeda SR (1996). Voltage-dependent modulation of N-type calcium channels by G-protein $\beta\gamma$ subunits. *Nature* **380**, 255–258.

Ishihara A, Ohira Y, Tanaka M, Nishikawa W, Ishioka N, Higashibata A, Izumi R, Shimazu T & Ibata Y (2001). Cell body size and succinate dehydrogenase activity of spinal motoneurons innervating the soleus muscle in mice, rats, and cats. *Neurochem Res* **26**, 1301–1304.

Ishii TM, Maylie J & Adelman JP (1997). Determinants of apamin and *d*-tubocurarine block in SK potassium channels. *J Biol Chem* **272**, 23195–23200.

Jeong SW, Ikeda SR & Wurster RD (1999). Activation of various G-protein coupled receptors modulates Ca^{2+} channel currents via PTX-sensitive and voltage-dependent pathways in rat intracardiac neurons. *J Auton Nerv Syst* **76**, 68–74.

Johnson IP (1986). A quantitative ultrastructural comparison of alpha and gamma motoneurons in the thoracic region of the spinal cord of the adult cat. *J Anat* **147**, 55–72.

Kemm RE & Westbury DR (1978). Some properties of spinal γ-motoneurones in the cat, determined by micro-electrode recording. *J Physiol* **282**, 59–71.

Kernell D (1999). Repetitive impulse firing in motoneurons: facts and perspectives. *Prog Brain Res* **123**, 31–37.

Khanna R, Roy L, Zhu X & Schlichter LC (2001). K^+ channels and the microglial respiratory burst. *Am J Physiol Cell Physiol* **280**, C796–C806.

Kohler M, Hirschberg B, Bond CT, Kinzie JM, Marrion NV, Maylie J & Adelman JP (1996). Small-conductance, calcium-activated potassium channels from mammalian brain. *Science* **273**, 1709–1714.

Lagerbäck PA (1985). An ultrastructural study of cat lumbosacral gamma-motoneurons after retrograde labelling with horseradish peroxidase. *J Comp Neurol* **240**, 256–264.

Lagerbäck PA, Cullheim S & Ulfhake B (1986). Electron microscopic observations on the synaptology of cat sciatic γ-motoneurons after intracellular staining with horseradish peroxidase. *Neurosci Lett* **70**, 23–27.

Lape R & Nistri A (2000). Current and voltage clamp studies of the spike medium afterhyperpolarization of hypoglossal motoneurons in a rat brain stem slice preparation. *J Neurophysiol* **83**, 2987–2995.

Li X & Bennett DJ (2007). Apamin-sensitive calcium-activated potassium currents (SK) are activated by persistent calcium currents in rat motoneurons. *J Neurophysiol* **97**, 3314–3330.

Lin MT, Lujan R, Watanabe M, Adelman JP & Maylie J (2008). SK2 channel plasticity contributes to LTP at Schaffer collateral–CA1 synapses. *Nat Neurosci* **11**, 170–177.

Lujan R, Maylie J & Adelman JP (2009). New sites of action for GIRK and SK channels. *Nat Rev Neurosci* **10**, 475–480.

McLarnon, JG (1995). Potassium currents in motoneurones. *Prog Neurobiol* **47**(6), 513–531.

© 2012 The Authors. The Journal of Physiology © 2012 The Physiological Society

McPhail LT, McBride CB, McGraw J, Steeves JD & Tetzlaff W (2004). Axotomy abolishes NeuN expression in facial but not rubrospinal neurons. *Exp Neurol* **185**, 182–190.

Maingret F, Coste B, Hao J, Giamarchi A, Allen D, Crest M, Litchfield DW, Adelman JP & Delmas P (2008). Neurotransmitter modulation of small-conductance Ca^{2+}-activated K^+ channels by regulation of Ca^{2+} gating. *Neuron* **59**, 439–449.

Manuel M, Meunier C, Donnet M & Zytnicki D (2005). How much afterhyperpolarization conductance is recruited by an action potential? A dynamic-clamp study in cat lumbar motoneurons. *J Neurosci* **25**, 8917–8923.

Mendell LM (2005). The size principle: a rule describing the recruitment of motoneurons. *J Neurophysiol* **93**, 3024–3026.

Meunier C & Borejsza K (2005). How membrane properties shape the discharge of motoneurons: a detailed analytical study. *Neural Comput* **17**, 2383–2420.

Miles GB, Dai Y & Brownstone RM (2005). Mechanisms underlying the early phase of spike frequency adaptation in mouse spinal motoneurones. *J Physiol* **566**, 519–532.

Miles GB, Hartley R, Todd AJ & Brownstone RM (2007). Spinal cholinergic interneurons regulate the excitability of motoneurons during locomotion. *Proc Natl Acad Sci U S A* **104**, 2448–2453.

Misonou H, Mohapatra DP, Park EW, Leung V, Zhen D, Misonou K, Anderson AE & Trimmer JS (2004). Regulation of ion channel localization and phosphorylation by neuronal activity. *Nat Neurosci* **7**, 711–718.

Mohapatra DP, Misonou H, Sheng-Jun P, Held JE, Surmeier DJ & Trimmer JS (2009). Regulation of intrinsic excitability in hippocampal neurons by activity-dependent modulation of the Kv2.1 potassium channel. *Channels* **3**:1, 46–56.

Monaghan AS, Benton DC, Bahia PK, Hosseini R, Shah YA, Haylett DG & Moss GW (2004). The SK3 subunit of small conductance Ca^{2+}-activated K^+ channels interacts with both SK1 and SK2 subunits in a heterologous expression system. *J Biol Chem* **279**, 1003–1009.

Mongan LC, Hill MJ, Chen MX, Tate SN, Collins SD, Buckby L & Grubb BD (2005). The distribution of small and intermediate conductance calcium-activated potassium channels in the rat sensory nervous system. *Neuroscience* **131**, 161–175.

Moschovakis AK, Burke RE & Fyffe RE (1991). The size and dendritic structure of HRP-labeled gamma motoneurons in the cat spinal cord. *J Comp Neurol* **311**, 531–545.

Muennich EA & Fyffe RE (2004). Focal aggregation of voltage-gated, Kv2.1 subunit-containing, potassium channels at synaptic sites in rat spinal motoneurones. *J Physiol* **554**, 673–685.

Mullen RJ, Buck CR & Smith AM (1992). NeuN, a neuronal specific nuclear protein in vertebrates. *Development* **116**, 201–211.

Piehl F, Arvidsson U, Hökfelt T & Cullheim S (1993). Calcitonin gene-related peptide-like immunoreactivity in motoneuron pools innervating different hind limb muscles in the rat. *Exp Brain Res* **96**, 291–303.

Power JM & Sah P (2008). Competition between calcium-activated K^+ channels determines cholinergic action on firing properties of basolateral amygdala projection neurons. *J Neurosci* **28**, 3209–3220.

Powers RK & Binder MD (2000). Relationship between the time course of the afterhyperpolarization and discharge variability in cat spinal motoneurones. *J Physiol* **528**, 131–150.

Powers RK, Sawczuk A, Musick JR & Binder MD (1999). Multiple mechanisms of spike-frequency adaptation in motoneurones. *J Physiol Paris* **93**, 101–114.

Prather JF, Nardelli P, Nakanishi ST, Ross KT, Nichols TR, Pinter MJ & Cope TC (2011). Recovery of proprioceptive feedback from nerve crush. *J Physiol* **589**, 4935–4947.

Ren Y, Barnwell LF, Alexander JC, Lubin FD, Adelman JP, Pfaffinger PJ, Schrader LA & Anderson AE (2006). Regulation of surface localization of the small conductance Ca^{2+}-activated potassium channel, Sk2, through direct phosphorylation by cAMP-dependent protein kinase. *J Biol Chem* **281**, 11769–11779.

Sah P & Faber ES (2002). Channels underlying neuronal calcium-activated potassium currents. *Prog Neurobiol* **66**, 345–353.

Sailer CA, Kaufmann WA, Marksteiner J & Knaus HG (2004). Comparative immunohistochemical distribution of three small-conductance Ca^{2+}-activated potassium channel subunits, SK1, SK2, and SK3 in mouse brain. *Mol Cell Neurosci* **26**, 458–469.

Santafé MM, Lanuza MA, Garcia N & Tomàs J (2006). Muscarinic autoreceptors modulate transmitter release through protein kinase C and protein kinase A in the rat motor nerve terminal. *Eur J Neurosci* **23**, 2048–2056.

Sarnat HB, Nochlin D & Born DE (1998). Neuronal nuclear antigen (NeuN): a marker of neuronal maturation in early human fetal nervous system. *Brain Dev* **20**, 88–94.

Sawczuk A, Powers RK & Binder MD (1997). Contribution of outward currents to spike-frequency adaptation in hypoglossal motoneurons of the rat. *J Neurophysiol* **78**, 2246–2253.

Schwindt PC, Spain WJ & Crill WE (1992). Calcium-dependent potassium currents in neurons from cat sensorimotor cortex. *J Neurophysiol* **67**, 216–226.

Seburn KL & Cope TC (1998). Short-term afferent axotomy increases both strength and depression at Ia–motoneuron synapses in rat. *J Neurosci* **18**, 1142–1147.

Shah M & Haylett DG (2000). The pharmacology of hSK1 Ca^{2+}-activated K^+ channels expressed in mammalian cell lines. *Br J Pharmacol* **129**, 627–630.

Shapiro MS, Loose MD, Hamilton SE, Nathanson NM, Gomeza J, Wess J & Hille B (1999). Assignment of muscarinic receptor subtypes mediating G-protein modulation of Ca^{2+} channels by using knockout mice. *Proc Natl Acad Sci U S A* **96**, 10899–10904.

Shneider NA, Brown MN, Smith CA, Pickel J & Alvarez FJ (2009). Gamma motor neurons express distinct genetic markers at birth and require muscle spindle-derived GDNF for postnatal survival. *Neural Dev* **4**, 42.

Skinner HJ, Girling KJ, Whitehurst A & Nathanson MH (1999). Influence of metoclopramide on plasma cholinesterase and duration of action of mivacurium. *Br J Anaesth* **82**, 542–545.

© 2012 The Authors. The Journal of Physiology © 2012 The Physiological Society

Stewart AE, Yan Z, Surmeier DJ & Foehring RC (1999). Muscarine modulates Ca^{2+} channel currents in rat sensorimotor pyramidal cells via two distinct pathways. *J Neurophysiol* **81**, 72–84.

Stocker M & Pedarzani P (2000). Differential distribution of three Ca^{2+}-activated K^+ channel subunits, SK1, SK2, and SK3, in the adult rat central nervous system. *Mol Cell Neurosci* **15**, 476–493.

Strassmaier T, Bond CT, Sailer CA, Knaus HG, Maylie J & Adelman JP (2005). A novel isoform of SK2 assembles with other SK subunits in mouse brain. *J Biol Chem* **280**, 21231–21236.

Strøbaek D, Jørgensen TD, Christophersen P, Ahring PK & Olesen SP (2000). Pharmacological characterization of small-conductance Ca^{2+}-activated K^+ channels stably expressed in HEK 293 cells. *Br J Pharmacol* **129**, 991–999.

Surmeier DJ & Foehring R (2004). A mechanism for homeostatic plasticity. *Nat Neurosci* **7**, 691–692.

Tacconi S, Carletti R, Bunnemann B, Plumpton C, Merlo Pich E & Terstappen GC (2001). Distribution of the messenger RNA for the small conductance calcium-activated potassium channel SK3 in the adult rat brain and correlation with immunoreactivity. *Neuroscience* **102**, 209–215.

Tiran Z, Peretz A, Attali B & Elson A (2003). Phosphorylation-dependent regulation of Kv2.1 channel activity at tyrosine 124 by Src and by protein-tyrosine phosphatase ε. *J Biol Chem* **278**, 17509–17514.

Viana F, Bayliss DA & Berger AJ (1993). Multiple potassium conductances and their role in action potential repolarization and repetitive firing behavior of neonatal rat hypoglossal motoneurons. *J Neurophysiol* **69**, 2150–2163.

Villalobos C, Shakkottai VG, Chandy KG, Michelhaugh SK & Andrade R (2004). SK_{Ca} channels mediate the medium but not the slow calcium-activated afterhyperpolarization in cortical neurons. *J Neurosci* **24**, 3537–3542.

Weyer A & Schilling K (2003). Developmental and cell type-specific expression of the neuronal marker NeuN in the murine cerebellum. *J Neurosci Res* **73**, 400–409.

Wilson JM, Rempel J & Brownstone RM (2004). Postnatal development of cholinergic synapses on mouse spinal motoneurons. *J Comp Neurol* **474**, 13–23.

Wolf HK, Buslei R, Schmidt-Kastner R, Schmidt-Kastner PK, Pietsch T, Wiestler OD & Blümcke I (1996). NeuN: a useful neuronal marker for diagnostic histopathology. *J Histochem Cytochem* **44**, 1167–1171.

Xia XM, Fakler B, Rivard A, Wayman G, Johnson-Pais T, Keen JE, Ishii T, Hirschberg B, Bond CT, Lutsenko S, Maylie J & Adelman JP (1998). Mechanism of calcium gating in small-conductance calcium-activated potassium channels. *Nature* **395**, 503–507.

Zagoraiou L, Akay T, Martin JF, Brownstone RM, Jessell TM & Miles GB (2009). A cluster of cholinergic premotor interneurons modulates mouse locomotor activity. *Neuron* **64**, 645–662.

Zengel JE, Reid SA, Sypert GW & Munson JB (1985). Membrane electrical properties and prediction of motor-unit type of medial gastrocnemius motoneurons in the cat. *J Neurophysiol* **53**, 1323–1344.

Zhang L & Krnjević K (1987). Apamin depresses selectively the after-hyperpolarization of cat spinal motoneurons. *Neurosci Lett* **74**, 58–62.

Zhou FM, Wilson C & Dani JA (2003). Muscarinic and nicotinic cholinergic mechanisms in the mesostriatal dopamine systems. *Neuroscientist* **9**, 23–36.

Author contributions

R.E.W.F. conceived and directed the experiments and interpreted data. R.E.W.F., A.S.D. and S.H.R. wrote the manuscript. S.H.R., A.S.D. and Z.D. performed immunohistochemistry, quantitative microscopic analysis and interpreted data; A.S.D. and K.L.B. collected electrophysiological data, filled cells and interpreted data; T.C.C. and P.N. directed electrophysiological experiments and analysis. Immunohistochemistry experiments and quantitative analysis were performed in the laboratory of R.E.W.F. Electrophysiological experiments were performed in the laboratory of T.C.C. T.C.C., P.N., K.L.B. and Z.D. all critically reviewed the manuscript for important intellectual content. We confirm all authors approve final version of the manuscript.

Acknowledgements

The authors thank Lori Goss for her excellent surgical work for the *in vivo* electrophysiological experiments as well as for the surgical work for the intramuscular injections of retrograde tracer. In addition, we thank Drs Francisco Alvarez, Mark Rich, Kathrin Engisch, David Ladle and Patrick Sonner for their helpful discussions and insights during the development of the project and the preparation of this manuscript. This work was funded by National Institute of Neurological Disorders and Stroke Program Project Grant P01-NS-057228.

© 2012 The Authors. The Journal of Physiology © 2012 The Physiological Society